RESEARCH ARTICLE

The centriole protein CEP76 negatively regulates PLK1 activity in the cytoplasm for proper mitotic progression

Yutaka Takeda, Kaho Yamazaki, Kaho Hashimoto, Koki Watanabe, Takumi Chinen*,‡ and Daiju Kitagawa*,‡

ABSTRACT

Polo-like kinase 1 (PLK1) dynamically changes its localization and plays important roles in proper mitotic progression. In particular, strict control of cytoplasmic PLK1 is needed to prevent mitotic defects. However, the regulation of cytoplasmic PLK1 is not fully understood. In this study, we show that CEP76, a centriolar protein, physically interacts with PLK1 and tightly controls the activation of cytoplasmic PLK1 during mitosis in human cells. We found that removal of centrosomes induced ectopic aggregation of PLK1, which is highly phosphorylated, in the cytoplasm during mitosis. Importantly, a targeted RNAi screen revealed that depletion of CEP76 resulted in a similar phenotype. In addition, depletion of CEP76 caused defective spindle orientation and mitotic delay. Moreover, the formation of ectopic PLK1 aggregates and defective spindle orientation were significantly suppressed by the inhibition of PLK1 kinase activity. Overall, these results demonstrate that CEP76 suppresses the aberrant activation of cytoplasmic PLK1 for proper mitotic progression.

This article has an associated First Person interview with the first author of the paper.

KEY WORDS: CEP76, PLK1, Centrosome, Centriole, Mitosis, Spindle

INTRODUCTION

The serine/threonine protein kinase, polo-like kinase 1 (PLK1) is an essential regulator of mitotic progression (Golsteyn, 1995). PLK1 was originally identified as the *polo* gene in *Drosophila melanogaster* (Llamazares et al., 1991; Sunkel and Glover, 1988) and is evolutionarily conserved from yeast to human (de Cárcer et al., 2011; Mulvihill et al., 1999). PLK1 dynamically changes its localization and regulates mitotic spindle organization for proper chromosome segregation (Barr et al., 2004). At the G2-M transition, PLK1 localizes at centrosomes and promotes centrosome maturation (Schmucker and Sumara, 2014). During prometaphase and metaphase, PLK1 at kinetochores regulates proper kinetochore–microtubule attachments, while PLK1 at centrosomes coordinates spindle positioning through the regulation of cortical dynein (Barr et al., 2004). At the onset of anaphase, PLK1 localizes to the central spindle and regulates midbody formation for proper cytokinesis (Barr et al., 2004). Therefore, the spatial and temporal transitions of PLK1

are important for accurate mitotic progression (Golsteyn, 1995; Schmucker and Sumara, 2014). Several factors regulate PLK1 localization during mitosis. PLK1 is recruited to centrosomes in a CDK1-dependent manner (Lee et al., 2014). The initial recruitment of PLK1 to kinetochores is mediated by its interaction with PBIP1 (also known as CENPU; Kang et al., 2006). During anaphase, PLK1 binds to PRC1 and changes its localization to the midbody (Hu et al., 2012). In addition, strict control of PLK1 in the cytoplasm is needed to prevent its aggregation and mitotic defects (Mukhopadhyay and Dasso, 2010; Schmit et al., 2012; Zhao et al., 2016). However, the detailed mechanisms through which the localization, expression and activity of PLK1 in mitosis are regulated are not fully understood.

The centrosome is a highly conserved membraneless organelle composed of one or two centrioles and surrounding pericentriolar material (PCM) (Conduit et al., 2015). Centrosomes act as a major microtubule-organizing center (MTOC), thereby ensuring proper mitotic progression. Therefore, it has been suggested that substantial gene mutations of centrosomal proteins are a cause of cancer and genetic disorders, such as microcephaly (Gönczy, 2015; Nigg and Raff, 2009). Centrosomes undergo multiple events during the cell cycle, such as centriole duplication, PCM expansion, centriole disengagement and subsequent daughter-to-mother centriole conversion. PLK1 has critical functions in these processes of centrosome regulation. After centriole duplication, the process of centrosome maturation is initiated with an extreme expansion of PCM in G2 phase (Kumar et al., 2016). During PCM expansion, CEP192 recruits Aurora A (AURKA) and PLK1 to centrosomes in a pericentrin-dependent (PCNT-dependent) manner, and subsequently activates these kinases to promote microtubule nucleation (Joukov et al., 2014). PLK1 phosphorylates PCNT to further recruit other PCM components onto centrosomes, thereby enhancing the microtubule nucleation activity of the centrosomes during mitosis (Lee and Rhee, 2011). Centriole disengagement occurring during anaphase in a separase (ESPL1)-dependent manner allows centrosomes to duplicate in the next cell cycle. In turn, the disengaged daughter centriole undergoes the process of daughter-to-mother centriole conversion (Tsou and Stearns, 2006; Vidwans et al., 1999). PLK1 is critical for both processes of centriole disengagement and conversion (Tsou et al., 2009). Although the mitotic functions of PLK1 in the regulation of centrosomes have been investigated in detail, the effects of centrosomes on the accurate regulation of PLK1 are not fully understood.

In this study, through removal of centrosomes and small-scale siRNA screening that targeted centrosomal proteins, we found that CEP76 suppressed the aberrant activation and ectopic aggregation of cytoplasmic PLK1 during mitosis. Depletion of CEP76 induced ectopic PLK1 aggregation in the cytoplasm, defective spindle orientation and mitotic delay in human cells. We also confirmed a physical interaction between PLK1 and CEP76. Moreover, the formation of PLK1 aggregates and defective spindle orientation depended on the kinase activity of PLK1. Thus, our results suggest that, in mitosis, CEP76 suppresses the

Department of Physiological Chemistry, Graduate School of Pharmaceutical Science, The University of Tokyo, Bunkyo, Tokyo 113-0033, Japan.

*These authors contributed equally to this work

‡Authors for correspondence (takumi.chinen@mol.f.u-tokyo.ac.jp; dkitagawa@mol.f.u-tokyo.ac.jp)

D.K., 0000-0003-2509-5977

aberrant activation of PLK1 in the cytoplasm to ensure proper mitotic progression.

RESULTS

Removal of centrosomes induces aberrant activation and ectopic aggregation of PLK1

To reveal the effects of centrosomes on the localization and phosphorylation status of PLK1 during mitosis, we initially observed PLK1 in fixed HeLa cells upon removal of centrosomes. Centrosomes can be eliminated from human cultured cells through inhibition or depletion of critical factors for centriole duplication, such as PLK4 (Habedanck et al., 2005) and STIL (Stevens et al., 2010). Owing to its simplicity, we depleted centrosomes from HeLa

cells through inhibition of PLK4 using centrinone, a PLK4-specific inhibitor (Wong et al., 2015). In control cells treated with dimethyl sulfoxide (DMSO), PLK1 was localized at centrosomes and kinetochores during mitosis, as previously described (Golsteyn, 1995). In contrast, PLK1 showed abnormal localization in mitotic cells treated with 100 nM centrinone (Fig. 1A). Specifically, the number of ectopic aggregates of PLK1, which were formed in the cytoplasm, dramatically increased in the mitotic cells without centrosomes (Fig. 1B).

Removal of centrosomes increased the number of cells that formed monopolar spindles in mitosis. It is possible that the ectopic aggregation of PLK1 was caused by an indirect effect due to bipolar spindle formation defects. Therefore, we examined whether
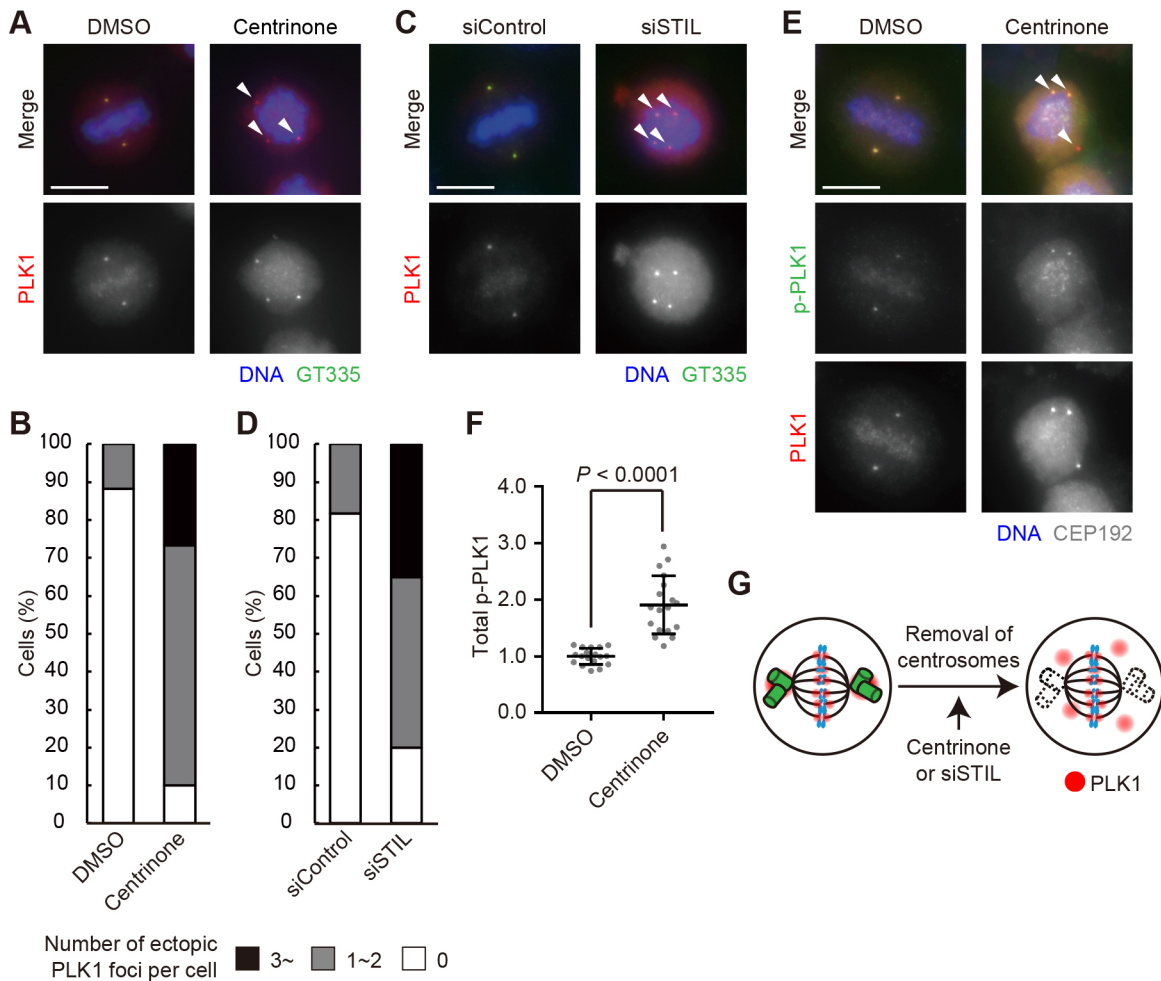

Fig. 1. Aberrant activation and ectopic aggregation of PLK1 in the cytoplasm upon removal of centrosomes. (A,B) HeLa cells were treated with dimethyl sulfoxide (DMSO; negative control; 0.1%) or centrinone (a PLK4 inhibitor; 100 nM) and immunostained with antibodies against polyglutamylation modification (GT335; green) and PLK1 (red). DNA was stained with Hoechst 33258 (blue). (A) Representative images of cells treated with DMSO or centrinone. Arrowheads indicate the ectopic aggregates of PLK1. Maximum intensity z-projections of 31 sections, every 1.0 μm. Scale bar: 10 μm. (B) The cells in each group were categorized into three patterns according to the number of ectopic aggregates of PLK1 per cell. N=60 cells from two independent experiments (N=30 per experiment). In the centrinone-treated cells, those without centrosomes (GT335 foci) were selected. (C,D) HeLa cells were treated with siControl or siSTIL, and immunostained with antibodies against GT335 (green) and PLK1 (red). DNA was stained with Hoechst 33258 (blue). (C) Representative images of the cells treated with siControl or siSTIL. Arrowheads indicate the ectopic aggregates of PLK1. Maximum intensity z-projections of 21 sections, every 0.5 μm. Scale bar: 10 μm. (D) The cells in each group were categorized into three patterns according to the number of ectopic aggregates of PLK1 per cell. N=60 cells from two independent experiments (N=30 per experiment). In the STIL-knockdown cells, those without centrosomes (GT335 foci) were selected. (E,F) HeLa cells were treated with DMSO or centrinone, and immunostained with antibodies against pT210-PLK1 (green), PLK1 (red) and CEP192 (gray). DNA was stained with Hoechst 33258 (blue). (E) Representative images of the cells treated with DMSO or centrinone. Arrowheads indicate the ectopic aggregates of PLK1. Maximum intensity z-projections of 21 sections, every 0.5 μm. Scale bar: 10 μm. (F) The total amount of p-PLK1 signal in a mitotic cell was quantified (sum of slices z-projections of 21 sections, every 0.5 μm). In this quantification, the cells selected in E were used. Line and error bars denote the mean intensity±s.d., and a Mann–Whitney U-test (two-tailed) was used to obtain the indicated P value. N=18 cells from two independent experiments. (G) A schematic illustration of the phenotype of PLK1 dysregulation upon removal of centrosomes observed in the experiments. Without centrosomes, mitotic cells form ectopic aggregates of PLK1.

there was a correlation between the ectopic formation of PLK1 aggregates and the structure of mitotic spindles. The ectopic aggregates of PLK1 were observed in mitotic cells with both monopolar and bipolar spindle structures, indicating that the phenotype was not induced by defects in bipolar spindle formation (Fig. S1A,B). Furthermore, a similar phenotype of PLK1 aggregation was observed in centrosome-eliminated cells through depletion of STIL (Fig. 1C,D), confirming that this phenotype was not specific to the PLK4 inhibition itself, but was commonly observed upon removal of centrosomes.

It has been shown that the catalytic activity of PLK1 at centrosomes is enhanced by the phosphorylation of threonine 210 (T210) of PLK1 (Tsvetkov and Stern, 2005). Interestingly, in acentrosomal cells, aggregated PLK1 was stained with the antibody against phosphorylated PLK1 (pT210-PLK1), indicating that PLK1 is in an active state in the ectopic aggregates (Fig. 1E). We hypothesized that the total amounts of PLK1 and phosphorylated PLK1 were altered in acentrosomal mitotic cells. Therefore, we quantified the amounts of PLK1 and pT210-PLK1 in an entire mitotic cell without centrosomes using immunofluorescence analyses. These cells showed slightly higher expression of PLK1 than that of control cells with centrosomes (Fig. S1C), suggesting that removal of centrosomes causes defects in the regulation of PLK1 expression level. Furthermore, the total amount of phosphorylated PLK1 also increased in acentrosomal cells (Fig. 1F). Collectively, these data suggest that centrosomes are necessary for the accurate regulation of the localization and phosphorylation status of PLK1 in the cytoplasm of mitotic cells (Fig. 1G).

Depletion of CEP76 or CEP192 causes ectopic aggregation of PLK1

We hypothesized that a number of centrosomal proteins are crucial for suppression of ectopic aggregation of PLK1 in mitosis. To identify such factors, we performed a small-scale knockdown screen using RNAi. Centrosomes undergo multiple events throughout the cell cycle, such as centriole duplication, PCM expansion, centriole disengagement and daughter-to-mother centriole conversion (Conduit et al., 2015). In the small-scale screen using HeLa cells, we depleted 11 kinds of centrosomal proteins involved in each step of the centrosome cycle: CEP57, CEP76, CEP97, CEP135, CEP152, CEP192, CEP295, SAS6 (also known as SASS6), PCNT, ODF2 and CPAP (also known as CENPJ) (Cizmecioglu et al., 2010; Dictenberg et al., 1998; Doxsey et al., 1994; Dzhindzhev et al., 2010; Gomez-Ferreria et al., 2007; Hatch et al., 2010; Ishikawa et al., 2005; Joukov et al., 2010; Kim et al., 2019; Kitagawa et al., 2011; Kleylein-Sohn et al., 2007; Leidel et al., 2005; Lin et al., 2013; Schmidt et al., 2009; Tang et al., 2009; Tsang et al., 2009; Tsuchiya et al., 2016; Watanabe et al., 2019; Zhu et al., 2008). Then, the behavior of PLK1 during mitosis was observed in fixed cells using immunofluorescence.

The results of the screening revealed that only CEP76 or CEP192 knockdown led to drastic ectopic aggregation of PLK1 in the cytoplasm during mitosis, which was similar to the phenotype observed in the acentrosomal cells shown in Fig. 1A (CEP76, 2.65 foci on average; CEP192, 3.05 foci on average; Fig. 2A,B). Approximately half of the CEP76- or CEP192-depleted cells exhibited at least three ectopic aggregates of PLK1 in the cytoplasm (Fig. 2B). Statistical analysis confirmed that only CEP76 or CEP192 knockdown significantly increased the percentage of the cells with ectopic PLK1 aggregates (Fig. 2C). PLK1 aggregates induced by CEP76 or CEP192 knockdown appeared to phenocopy the removal of centrosomes (Fig. 1A–D); thus, we examined the link between these phenotypes. To this end, we tested the effect of

centrosome removal on the expression levels and spindle pole localization of CEP76 and CEP192. We quantified the total amount of CEP76 and CEP192 by western blotting, and confirmed the downregulation of the two proteins in acentrosomal cells (Fig. S1D–F). In addition, CEP76, CEP192 and PLK1 were not recruited to spindle poles without centrosomes (Fig. S1G–I). These data suggest that the ectopic PLK1 aggregation observed upon the removal of centrosomes was induced, at least partly, by downregulation of CEP76 and CEP192. Alternatively, it is also possible that CEP76 and CEP192 locally control the state of PLK1 at centrosomes. Collectively, this suggests that the two centrosomal proteins CEP76 and CEP192 are involved in the suppression of ectopic PLK1 aggregation in the cytoplasm during mitosis.

CEP76 is not essential for centriole duplication, recruitment of PLK1 to centrosomes or establishment of spindle bipolarity

It has been well established that CEP192 is crucial for centriole duplication, recruitment of PLK1 to centrosomes and subsequent bipolar spindle formation in mitosis (Joukov et al., 2014). In line with the findings of previous studies, depletion of CEP192 led to a decrease in the number of centrioles in our experimental conditions (Fig. 3A,B) and significantly reduced centrosomal loading of PLK1 (Fig. 3C,D). Furthermore, most of the CEP192-depleted cells exhibited mitotic arrest with monopolar spindles (Fig. S2A,B). Subsequently, we examined whether depletion of CEP76 caused similar phenotypes. In sharp contrast, CEP76-depleted cells did not exhibit the phenotypes observed in CEP192-depleted cells, such as the decrease in the number of centrioles, failure of recruitment of PLK1 to centrosomes or mitotic arrest with monopolar spindles (Fig. 3A–D; Fig. S2A,B). We also tested the mutual dependency of CEP76 and CEP192 on their localization at centrosomes and found that they were only partially dependent on each other in mitosis (Fig. 3E–H) and interphase (Fig. S2C–F). Collectively, these results suggest that CEP76 is not essential for centriole duplication, recruitment of PLK1 to centrosomes or establishment of spindle bipolarity.

CEP76 physically interacts with PLK1 and localizes at the distal ends of centrioles and the proximal ends of mother centrioles

To further address the relationship between CEP76, CEP192 and PLK1, we examined the physical interaction and localization of CEP76, CEP192 and PLK1 in human cells. CEP76 and CEP192 did not show any physical interaction in co-immunoprecipitation experiments with HEK293T cells (Fig. S3A), whereas PLK1 interacted with both CEP76 and CEP192 (Fig. 4A; Fig. S3B). These results raise a possibility that these three proteins do not form a ternary complex. Notably, PLK1 specifically interacted with CEP76 in a polo-box-domain-dependent manner (amino acids 310–603) (Fig. 4A). To further address the physical interaction between CEP76 and PLK1, we performed a yeast two-hybrid assay, and the interaction between the two proteins was also detected (Fig. 4B). Taken together, these data suggest that CEP76 physically interacts with and regulates PLK1.

Next, we used the Airyscan confocal microscopy system to observe mitotic centrosomes in fixed cells and revealed the detailed localization pattern of CEP76 at centrosomes. Using established centriolar markers (SAS6, a marker for the proximal ends of daughter centrioles; CEP152, a marker for the proximal ends of mother centrioles) as references, we found that CEP76 was localized at the distal and proximal ends of mother centrioles and the distal ends of daughter centrioles (Fig. 4C,D). The specificity of the
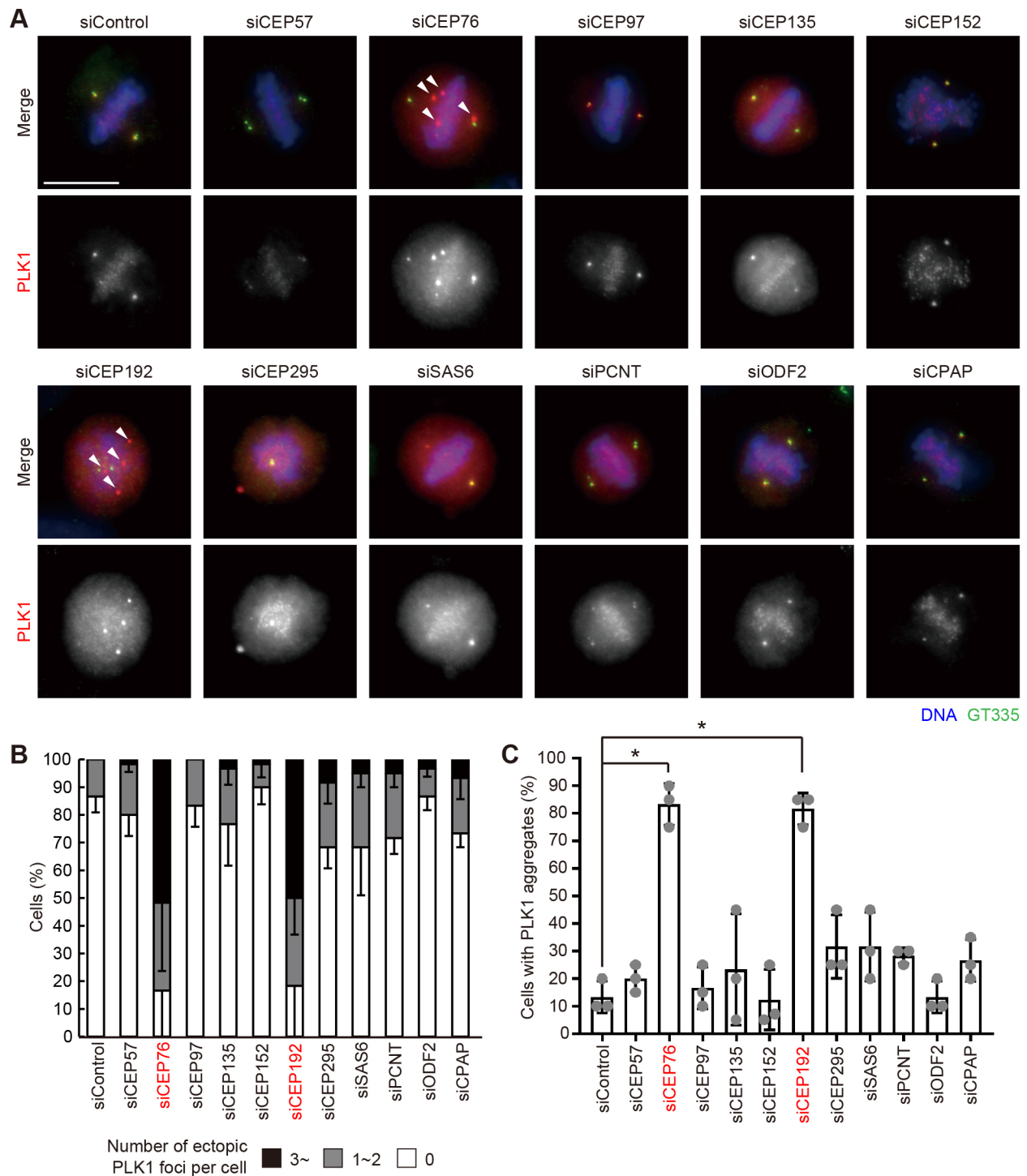
Fig. 2. Ectopic aggregation of PLK1 upon depletion of CEP76 or CEP192. (A–C) HeLa cells were treated with siControl, siCEP57, siCEP76, siCEP97, siCEP135, siCEP152, siCEP192, siCEP295, siSAS6, siPCNT, siODF2 or siCPAP, and immunostained with antibodies against polyglutamylation modification (GT335; green) and PLK1 (red). DNA was stained with Hoechst 33258 (blue). (A) Representative images of the cells treated with each siRNA. Arrowheads indicate the ectopic aggregates of PLK1. Maximum intensity z-projections of 21 sections, every 0.5 µm. Scale bar: 10 µm. (B) The cells in each group were categorized into three patterns according to the number of ectopic aggregates of PLK1 per cell. Values are presented as the mean percentage±s.d. from three independent experiments (N=20 cells per experiment). (C) Frequency of cells with ectopic PLK1 aggregation. In this statistical test, the values in B were used. Line and error bars denote the mean percentage±s.d. N=3 independent experiments. *P<0.05 (Kruskal–Wallis test).

antibody against CEP76 was confirmed by siRNA-mediated depletion of CEP76 (Fig. 4C). The same localization pattern of CEP76 was observed in a different manner, using canonical confocal microscopy, whereas PLK1 and CEP192 were observed to be

localized at the PCM surrounding the centriole wall (Fig. S3C,D). Overall, these data suggest that CEP76 and CEP192 independently interact with PLK1 and might regulate PLK1 at different positions in centrosomes during mitosis.
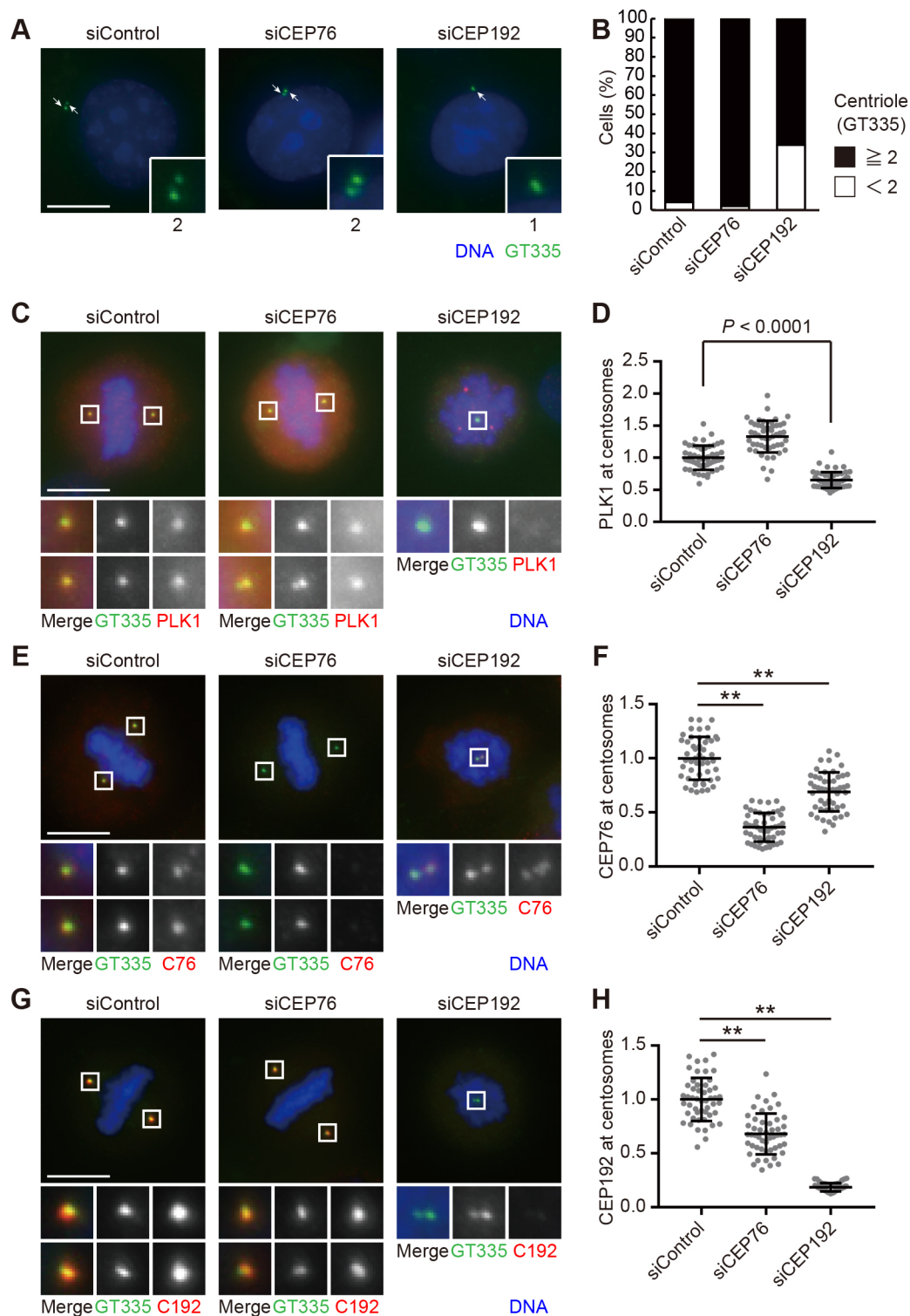
Fig. 3. See next page for legend.

Depletion of CEP76 induces highly phosphorylated PLK1 aggregates in early mitosis, followed by mitotic delay

It has been reported that CEP192 interacts with PLK1 and organizes the Aurora A–PLK1 cascade (Joukov et al., 2014). Considering that the function of CEP76 in the regulation of mitotic PLK1 is not well characterized, hereafter we focused on CEP76. Firstly, to confirm that the ectopic PLK1 aggregation in CEP76-depleted cells was not induced by off-target effects of the siRNA, we depleted CEP76

from HeLa cells through additional means. Cells treated with an siRNA targeting a different sequence within the CEP76 open reading frame (siCEP76#2) formed similar aggregates of PLK1 in mitosis (Fig. S4C,D). Moreover, when HeLa cells stably expressing Cas9 were transfected with sgCEP76 (as shown in Fig. S4E), a similar phenotype was observed (Fig. S4H,I). In these experiments, the efficiency of CEP76 depletion at centrioles was confirmed using an antibody against CEP76 (Fig. S4A,B,F,G). Furthermore, in a

Fig. 3. Comparison of phenotypes of CEP76- and CEP192-depletion.
(A,B) HeLa cells were treated with siControl, siCEP76 or siCEP192, and immunostained with an antibody against polyglutamylation modification (GT335; green). DNA was stained with Hoechst 33258 (blue).
(A) Representative images of interphase cells treated with siControl, siCEP76 or siCEP192. Arrows indicate the positions of the centrioles (shown enlarged in inset images). Maximum intensity z-projections of 21 sections, every 0.5 μm. Scale bar: 10 μm. (B) The cells in each group were categorized into two patterns according to the number of centrioles. N=50 cells. (C,D) HeLa cells were treated with siControl, siCEP76 or siCEP192, and immunostained with antibodies against GT335 (green) and PLK1 (red). DNA was stained with Hoechst 33258 (blue). (C) Representative images of the mitotic cells treated with siControl, siCEP76 or siCEP192. Maximum intensity z-projections of 21 sections, every 0.5 μm. Boxes indicate regions shown below in enlarged single-channel images. Scale bar: 10 μm. (D) Quantification of PLK1 intensity at centrosomes (GT335 foci) in the cells in each group. Line and error bars denote the mean intensity±s.d. and the Kruskal–Wallis test was used to obtain the indicated P value. N=50 centrosomes. (E,F) HeLa cells were treated with siControl, siCEP76 or siCEP192, and immunostained with antibodies against GT335 (green) and CEP76 (red). DNA was stained with Hoechst 33258 (blue). (E) Representative images of the mitotic cells treated with siControl, siCEP76 or siCEP192. C76 indicates CEP76. Maximum intensity z-projections of 21 sections, every 0.5 μm. Boxes indicate regions shown below in enlarged single-channel images. Scale bar: 10 μm. (F) Quantification of CEP76 intensity at centrosomes (GT335 foci) in the cells in each group. Line and error bars denote the mean intensity±s.d. N=50 centrosomes. **P<0.0001 (Kruskal–Wallis test). (G,H) HeLa cells were treated with siControl, siCEP76 or siCEP192, and immunostained with antibodies against GT335 (green) and CEP192 (red). DNA was stained with Hoechst 33258 (blue). (G) Representative images of the mitotic cells treated with siControl, siCEP76 or siCEP192. C192 indicates CEP192. Maximum intensity z-projections of 21 sections, every 0.5 μm. Boxes indicate regions shown below in enlarged single-channel images. Scale bar: 10 μm. (H) Quantification of CEP192 intensity at centrosomes (GT335 foci) in the cells in each group. Line and error bars denote the mean intensity±s.d. N=50 centrosomes. **P<0.0001 (Kruskal–Wallis test).

live-cell imaging analysis with HeLa cells expressing endogenously tagged PLK1–mCherry (Fig. 5A), we observed that ectopic PLK1 aggregates were gradually generated from early mitosis, upon depletion of CEP76 (Fig. 5B). These results confirmed that depletion of CEP76 causes ectopic aggregation of PLK1 in the cytoplasm during mitosis. We further observed that the ectopic aggregates of PLK1 were stained by the pT210-PLK1 antibody (Fig. 5E). The phenotype was similar to that of the cells without centrosomes, as shown in Fig. 1E. Although the intensity of the phosphorylated PLK1 at centrosomes did not change in CEP76-depleted cells (Fig. S7B), the total amount of the phosphorylated PLK1 in an entire mitotic cell was significantly increased (Fig. 5F). These data suggest that depletion of CEP76 mainly affects the phosphorylation state of PLK1 in the cytoplasm and causes ectopic aggregation of PLK1.

Next, we focused on the properties of the ectopic PLK1 aggregates in CEP76-depleted cells. Under several conditions, PLK1 aggregates recruit other PCM components and act as MTOCs (Zhao et al., 2016). To determine whether the ectopic PLK1 aggregates in CEP76-knockdown cells could recruit other PCM components, nucleate microtubules and act as spindle poles, we performed several experiments. Firstly, we confirmed that CEP76-knockdown cells with ectopic PLK1 aggregates formed bipolar spindles in mitosis (Fig. S5A,B). Secondly, we observed the localization of other PCM proteins (PCNT and NEDD1). Both proteins localized at centrosomes and were not recruited into the ectopic PLK1 aggregates in CEP76-knockdown cells (normal localization; Fig. S5C–F). Collectively, these data suggest that the aggregates do not act as extra spindle poles.

Next, using the live-cell imaging data, we analyzed in more detail the mitotic progression and PLK1 dynamics. CEP76-depleted cells showed significant mitotic delay compared with control cells. On average, control cells and CEP76-depleted cells completed cytokinesis in 56.1 and 86.9 min after the mitotic onset, respectively (Fig. 5C). However, the initiation of the ectopic aggregation of PLK1 in CEP76-depleted cells was markedly earlier than cytokinesis in control cells (Fig. 5D). Therefore, the mitotic delay in CEP76-depleted cells does not appear to be a cause of the ectopic aggregation of PLK1. These data suggest that depletion of CEP76 causes formation of the ectopic aggregates of PLK1 in the cytoplasm, which are highly phosphorylated, and subsequently induces mitotic delay in human cells.

Depletion of CEP76 causes defective spindle orientation
To reveal the biological significance of CEP76 in the context of PLK1 regulation during mitosis, we carefully compared the mitotic spindles of CEP76-depleted cells with those of control cells. Because PLK1 is a master regulator of spindle orientation in most animal cells (Hanafusa et al., 2015; Miyamoto et al., 2017; Sana et al., 2018; Yan et al., 2015), upon depletion of CEP76, we firstly quantified spindle orientation in mitotic HeLa cells. In this quantification, we judged the positions of spindle poles according to the centrin signal and calculated 'spindle angle' as previously described (Yan et al., 2015) (Fig. 6A). Interestingly, CEP76-depleted cells showed severe defects in spindle orientation (Fig. 6B,C). Spindle poles in CEP76-depleted cells were detected in markedly different z planes (Fig. 6B). These data suggest that CEP76 is important for the maintenance of spindle orientation during mitosis.

Next, to determine whether the aberrant activation of PLK1 exerts the same defect in spindle orientation, we generated a cell line for PLK1 overexpression (HeLa Tet-On-PLK1; Fig. 6D). The Tet-On system enabled us to gradually overexpress the PLK1 protein, depending on the concentration of doxycycline (Dox) in the culture medium. Titration of Dox concentration revealed that treatment with 100 ng/ml Dox was sufficient to upregulate the level of PLK1 expression and induce ectopic PLK1 aggregation (Fig. S6A–C). Using the HeLa Tet-On-PLK1 cells, we found that the PLK1 overexpression induced by 100 ng/ml Dox caused defective spindle orientation in mitosis, which was similar to the phenotype observed in CEP76-depleted cells (Fig. 6E,F; Fig. S6D). Collectively, depletion of CEP76 and overexpression of PLK1 similarly cause spindle orientation defects in mitotic HeLa cells.

Ectopic formation of PLK1 aggregates and spindle orientation defects depend on PLK1 kinase activity in CEP76-depleted cells
To verify whether the kinase activity of PLK1 is important for the phenotypes induced by depletion of CEP76, we performed rescue experiments by treating CEP76-knockdown cells with BI 2536, a PLK1-specific inhibitor (Steegmaier et al., 2007), and observed PLK1 localization and spindle orientation (Fig. S7A). As mentioned above, the phosphorylation of PLK1 at T210 is required for the activation of PLK1. Following treatment with BI 2536, the intensity of phosphorylated PLK1 at centrosomes was dramatically decreased (Fig. S7C,D), confirming that the experimental procedure was suitable to inhibit the activation of PLK1. Interestingly, treatment with BI 2536 suppressed the ectopic aggregation of PLK1 in CEP76-depleted cells (final concentration of 10 nM; Fig. 7A,B). In addition, we quantified the total amount of PLK1 in mitotic cells. To focus on only mitotic cells, we observed fixed mitotic cells using
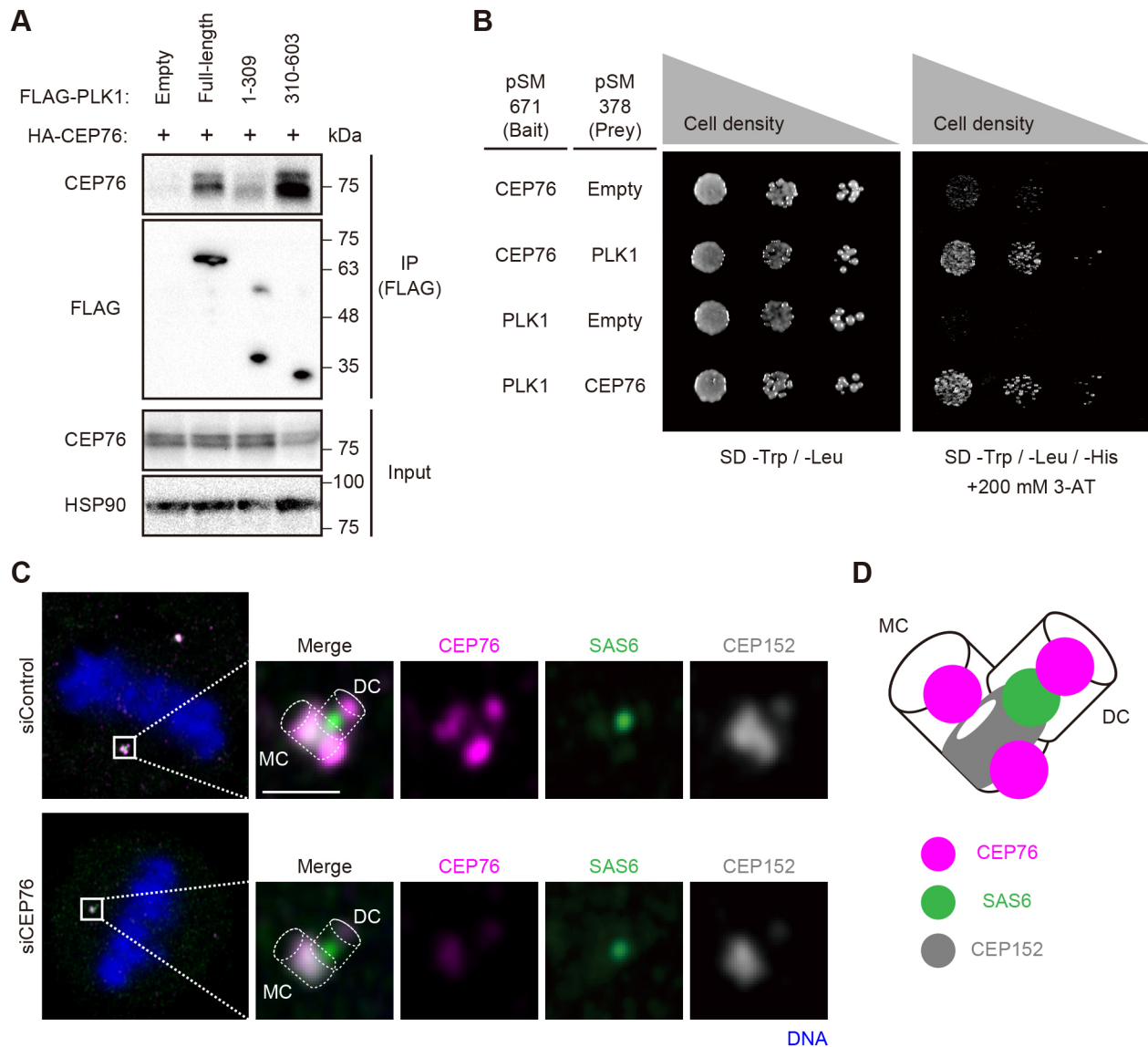
Fig. 4. Physical interaction between CEP76 and PLK1, and precise localization of CEP76 at centrioles. (A) HEK293T cells co-expressing FLAG-Empty (negative control) or FLAG–PLK1 (full-length or the indicated amino acid fragments), and HA–CEP76 were immunoprecipitated with an antibody against the FLAG tag. The samples were blotted and examined using antibodies against CEP76, FLAG tag or HSP90. (B) Yeast two-hybrid assay showing the interaction between CEP76 and PLK1. The indicated clones were grown on plates with SD medium lacking tryptophan, leucine and histidine, with 200 mM 3-Amino-1,2,4-triazole (3-AT) at 30°C. (C) HeLa cells were treated with siControl or siCEP76, and immunostained with antibodies against CEP76 (magenta), SAS6 (a marker for the proximal ends of daughter centrioles; green) and CEP152 (a marker for the proximal ends of mother centrioles; gray). DNA was stained with Hoechst 33258 (blue). Representative images of the cells are shown with boxes indicating the regions shown in enlarged single-channel images. MC and DC indicate mother and daughter centrioles, respectively. Single slice. Scale bar: 1.0 µm. (D) A schematic illustration of the localization of CEP76 at centrosomes observed in C. Magenta, green and gray indicate CEP76, SAS6 and CEP152, respectively.

immunofluorescence. The amount of PLK1 in CEP76-depleted cells was slightly increased compared with that measured in control cells; this result was similar to that for cells without centrosomes, as shown in Fig. S1C (Fig. S7E). Treatment with BI 2536 decreased the amount of PLK1 in an entire mitotic cell, although the phenotype was not completely rescued (Fig. S7E). We also tried to quantify the total amount of PLK1 by western blotting of whole-cell lysates, but we were not able to detect a significant difference between control and CEP76-depleted cells (Fig. S7F). Most of these lysates were derived from interphase cells, which is consistent with the observation that PLK1 expression level in interphase of CEP76-depleted cells was comparable to that of control cells (Fig. S7G). Overall, the kinase activity of PLK1 is necessary for its ectopic aggregation in mitosis.

Furthermore, we verified that the spindle orientation defects in CEP76-depleted cells were also suppressed by inhibition of PLK1. We treated CEP76-knockdown cells with BI 2536 and calculated the 'spindle angle' in mitosis. In this experiment, a low concentration of BI 2536 was used to avoid the effects on the establishment of spindle bipolarity (final concentration of 3 nM). The spindle orientation defects in CEP76-depleted cells were mildly suppressed by treatment with BI 2536 (Fig. 7C,D). These data suggest that the spindle orientation defects in CEP76-knockdown cells are also dependent on the kinase activity of PLK1. Collectively, this suggests that the phenotypes observed in CEP76-depleted cells, namely ectopic PLK1 aggregates and spindle orientation defects, are induced by aberrant activation of PLK1.
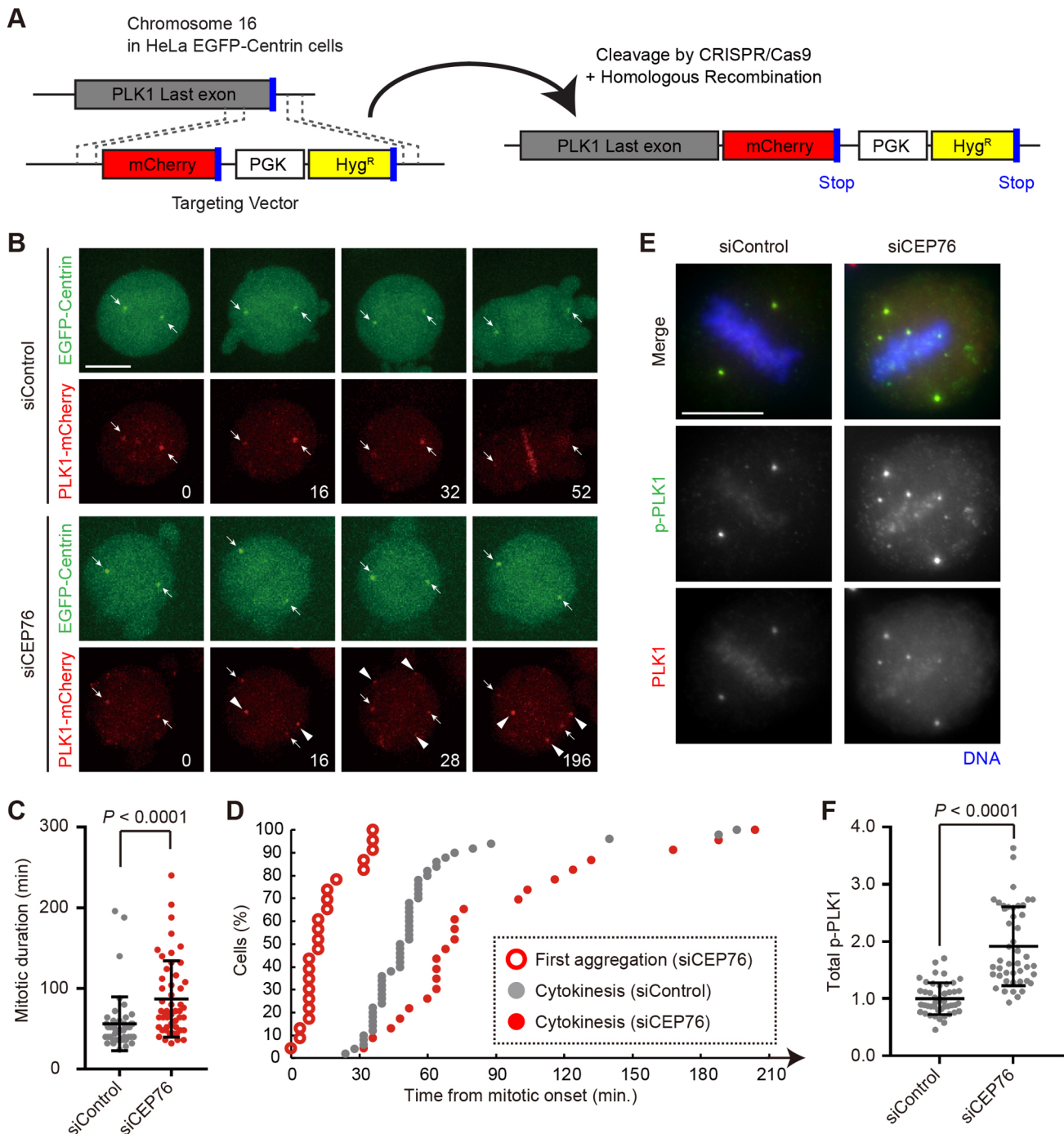
Fig. 5. Aggregation of phosphorylated PLK1 in early mitosis, which is followed by mitotic delay. (A) Schematic illustration of the endogenous tagging system. Using the CRISPR/Cas9 system and drug selection for HeLa EGFP–centrin-1 cells, an mCherry sequence was inserted into the C terminus (exon 10) of PLK1. Hyg[R], hygromycin resistance sequence. (B–D) Time-lapse observation of endogenous PLK1 in mitotic cells treated with siControl or siCEP76. HeLa cells stably expressing EGFP–centrin-1 and PLK1–mCherry were observed with a 60× objective. (B) Representative images of the cells treated with siControl or siCEP76. Green and red represent EGFP–centrin-1 and PLK1–mCherry, respectively. Arrows indicate the positions of centrosomes and arrowheads indicate ectopic aggregates of PLK1. Time from mitotic onset is indicated (min). Maximum intensity z-projections of 20 sections, every 1.3 µm. Scale bar: 10 µm. (C) Quantification of the duration from mitotic onset to cytokinesis of the cells in each group in B. Line and error bars denote the mean time±s.d. and the Mann–Whitney U-test (two-tailed) was used to obtain the indicated P value. N=50 cells from two independent experiments (N=25 per experiment). (D) The time from mitotic onset to the first aggregation of PLK1 in CEP76-depleted cells and cytokinesis in control and CEP76-depleted cells. Each plot shows the cumulative percentage of each event at each time point for the cells shown in C. In the cells treated with siCEP76, those showing visible PLK1 aggregates in the cytoplasm were selected. siControl, N=total 50 cells; siCEP76, N=total 23 cells; taken from two independent experiments. (E,F) HeLa cells were treated with siControl or siCEP76, and immunostained with antibodies against pT210-PLK1 (green) and PLK1 (red). DNA was stained with Hoechst 33258 (blue). (E) Representative images of the cells treated with siControl or siCEP76. Maximum intensity z-projections of 21 sections, every 0.5 µm. Scale bar: 10 µm. (F) The total amount of p-PLK1 signal in a mitotic cell was quantified (sum of slices z-projections of 21 sections, every 0.5 µm). In this quantification, the cells imaged in E were used. Line and error bars denote the mean intensity±s.d. and the Mann–Whitney test (two-tailed) was used to obtain the indicated P value. N=45 cells from two independent experiments.
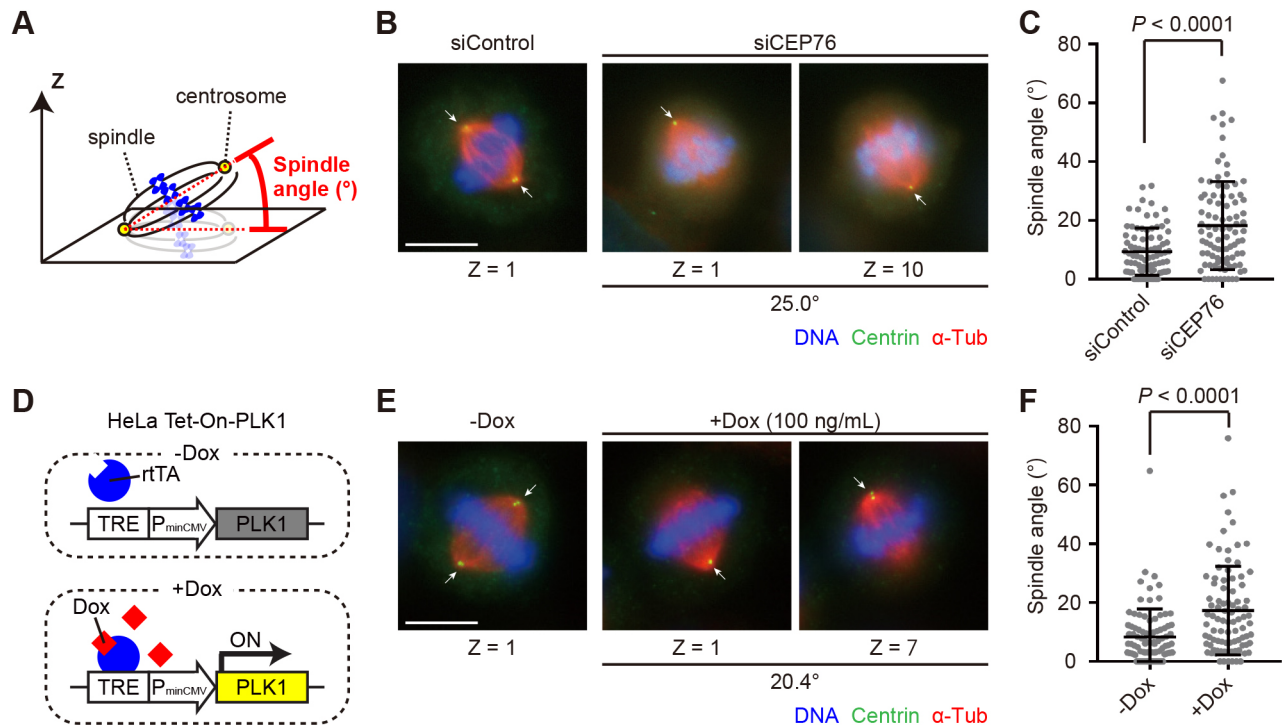
Fig. 6. Defective spindle orientation upon depletion of CEP76. (A) Schematic illustration showing the calculation of mitotic spindle orientation (spindle angle). (B,C) HeLa cells were treated with siControl or siCEP76, and immunostained with antibodies against centrin (green) and α-tubulin (red). DNA was stained with Hoechst 33258 (blue). (B) Representative images of the cells treated with siControl or siCEP76. Arrows indicate positions of centrosomes (spindle poles). Images are single slices, and the z-step shown is indicated. z-step, 0.5 µm. Scale bar: 10 µm. (C) Quantification of the spindle angle of the cells in each group. Line and error bars denote the mean angle±s.d. and the Mann–Whitney U-test (two-tailed) was used to obtain the indicated P value. siControl, N=total 90 cells; siCEP76, N=total 84 cells; taken from four independent experiments. (D) A schematic illustration of the Tet-On overexpression system. In HeLa Tet-On-PLK1 cells, titration of doxycycline (Dox) concentration allowed the regulation of the level of expression of PLK1, as shown in Fig. S6. (E,F) HeLa Tet-On-PLK1 cells were treated with Dox (100 ng/ml) or left untreated, and immunostained with antibodies against centrin (green) and α-tubulin (red). DNA was stained with Hoechst 33258 (blue). (E) Representative images of the cells treated with Dox (+Dox) or left untreated (–Dox). Arrows indicate the positions of centrosomes (spindle poles). Images are single slices, and the z-step shown is indicated, z-step, 0.5 µm. Scale bar: 10 µm. (F) Quantification of the spindle angle of the cells in each group. Line and error bars denote the mean angle±s.d. and the Mann–Whitney U-test (two-tailed) was used to obtain the indicated P value. N=90 cells from three independent experiments (N=30 per experiment).

DISCUSSION

The proper regulation of PLK1 is crucial for accurate chromosome segregation and cell cycle progression (Kumar et al., 2016). Previous reports have revealed transitions of PLK1 localization and functions during mitosis (Schmucker and Sumara, 2014). In this study, we showed that CEP76, a centriolar protein, is important for the regulation of PLK1 in mitotic human cells. Although the intensity of centrosomal pT210-PLK1 did not change (Fig. S7B), the total amount of pT210-PLK1 significantly increased in CEP76-depleted cells (Fig. 5F). A similar upregulation was observed in acentrosomal cells (Fig. 1F). These data suggest that CEP76 at centrioles suppresses the overactivation of PLK1 in the cytoplasm.

CEP76-depleted cells exhibited the formation of ectopic PLK1 aggregates in the cytoplasm (Fig. 8). Although similar observations of PLK1 aggregates in mitotic mammalian cells have already been reported by several groups, there are some differences when compared to the aggregates noted in CEP76-knockdown cells (Mukhopadhyay and Dasso, 2010; Schmit et al., 2012; Zhao et al., 2016). Mukhopadhyay and Dasso (2010) focused on inner kinetochore proteins (IKPs) and showed that the proper regulation of IKPs is important for avoiding PLK1 aggregation. However, according to our observations, CEP76 did not localize around kinetochores (Fig. 4C), suggesting that these phenotypes are the results of different mechanisms. Schmit et al. (2012) stated that mislocalization of PLK1 upon depletion of NUMB leads to

disorganized recruitment of centrosomal γ-tubulin. In CEP76-depleted cells, this defect was not observed, and PCM proteins were properly recruited into centrosomes (Fig. S5C–F). Zhao et al. (2016) reported that the cytosolic PLK1 aggregation in MLL5 (KMT2E)-depleted cells causes formation of extra MTOCs and multipolar spindles in mitosis. In our study, the PLK1 aggregates did not recruit other PCM components or significantly affect the establishment of spindle bipolarity (Fig. S5A–F). Moreover, Zhao et al. (2016) used U2OS cells in their study, but we could not observe ectopic PLK1 aggregation after CEP76 knockdown in U2OS cells (Fig. S8F,H). Overall, our observation of ectopic PLK1 aggregation in CEP76-depleted cells is novel, at least with these considerations.

How was the ectopic PLK1 aggregation induced in CEP76-depleted cells? A modest expression level of PLK1 (final Dox concentration of 10 ng/ml) did not induce the phenotypes observed in CEP76-depleted cells (e.g. ectopic PLK1 aggregation, spindle orientation defects) (Fig. S6B–D). Thus, the higher expression level of PLK1 itself does not explain the phenotypes resulting from the depletion of CEP76. CEP76 might directly influence the regulation of PLK1 kinase activity at centrioles. In this situation, the aberrantly activated PLK1 is immediately diffused into the cytoplasm, and the active PLK1 is somehow transformed into a stable state, forming ectopic aggregates of PLK1. However, the molecular mechanism through which CEP76 directly regulates PLK1 at centrioles remains
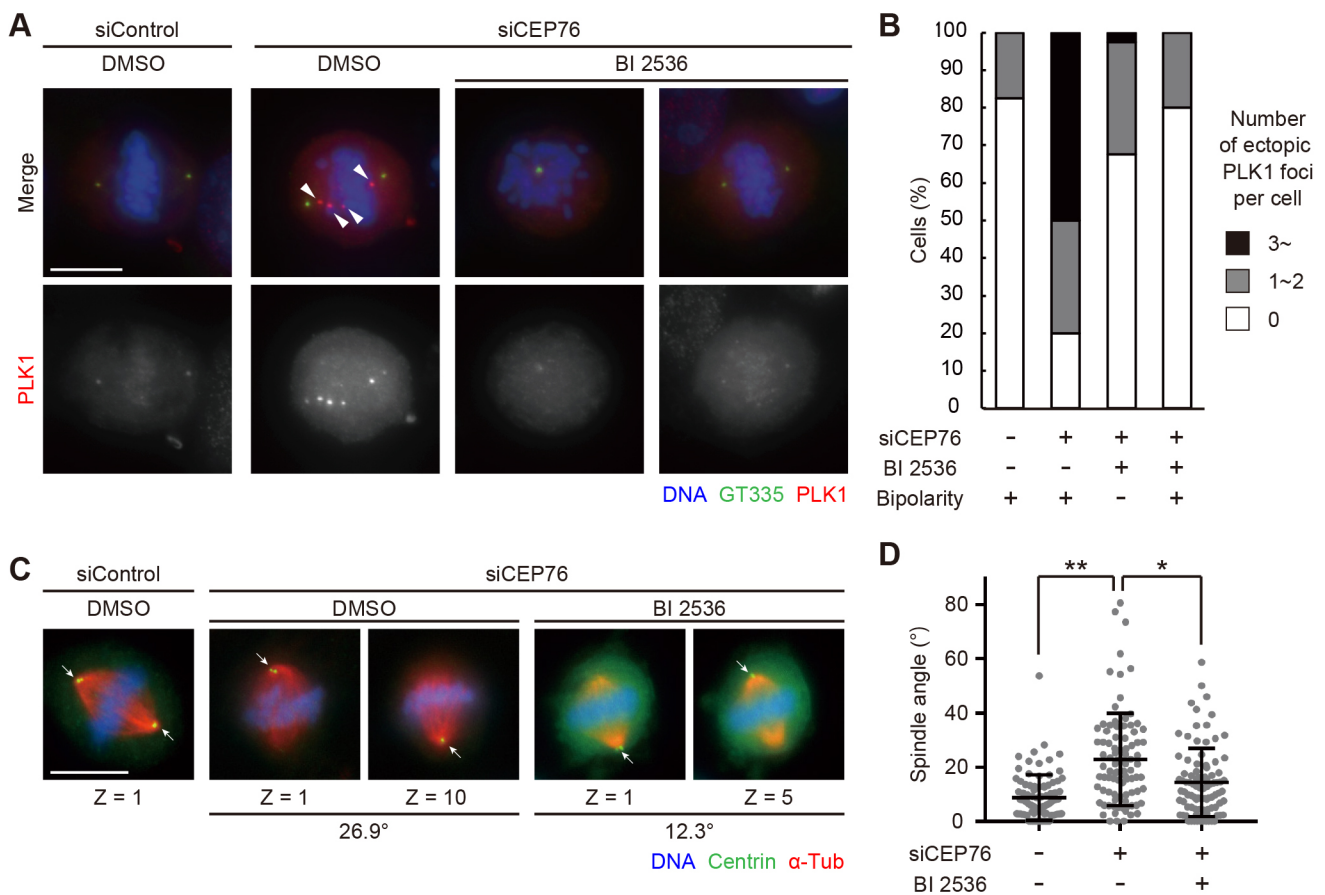
Fig. 7. Ectopic PLK1 aggregation and spindle orientation defects depending on PLK1 kinase activity in CEP76-depleted cells. (A,B) Control and CEP76-knockdown cells were treated with DMSO (0.1%) or BI 2536 (a PLK1 inhibitor; 10 nM) for 6 h, and immunostained with antibodies against polyglutamylation modification (GT335; green) and PLK1 (red). DNA was stained with Hoechst 33258 (blue). (A) Representative images of the cells in each group. Arrowheads indicate the ectopic aggregates of PLK1. Maximum intensity z-projections of 21 sections, every 0.5 µm. Scale bar: 10 µm. (B) The cells in each group were categorized into three patterns according to the number of ectopic aggregates of PLK1 per cell. N=40 cells from two independent experiments (N=20 per experiment). The CEP76-knockdown cells treated with BI 2536 were divided into two groups according to the mitotic spindle structures, monopolar or bipolar. (C,D) Control and CEP76-knockdown cells were treated with DMSO (0.1%) or BI 2536 (3 nM) for 6 h, and immunostained with antibodies against centrin (green) and α-tubulin (red). DNA was stained with Hoechst 33258 (blue). (C) Representative images of the cells in each group. Arrows indicate the positions of centrosomes (spindle poles). Images are single slices, with the z-step indicated below. z-step, 0.5 µm. Scale bar: 10 µm. (D) Quantification of the spindle angle of the cells in each group. Line and error bars denote the mean angle±s.d. N=90 cells from three independent experiments (N=30 per experiment). **P<0.0001, *P<0.05 (Kruskal–Wallis test).

unclear. Thus, further study is needed to understand the detailed interaction between CEP76 and PLK1. Bora and Aurora A activate PLK1 in mitosis (Bruinsma et al., 2014). Therefore, these factors and CEP76 might be involved together in the regulation of PLK1 activation.

In addition, we found that depletion of CEP76 also caused severe spindle orientation defects in mitosis. Spindle orientation is important for tissue morphogenesis, asymmetric cell division and

stem cell self-renewal (Knoblich, 2010; Lu and Johnston, 2013; Siller and Doe, 2009). This phenotype was rescued by inhibition of PLK1, similar to the ectopic PLK1 aggregation. These results suggest that CEP76-dependent suppression of aberrant PLK1 activation is important to ensure proper spindle orientation. PLK1 is a key factor for maintaining spindle orientation during mitosis. Previous studies have shown that the kinase activity of PLK1 is necessary for spindle positioning, and that inhibition of PLK1
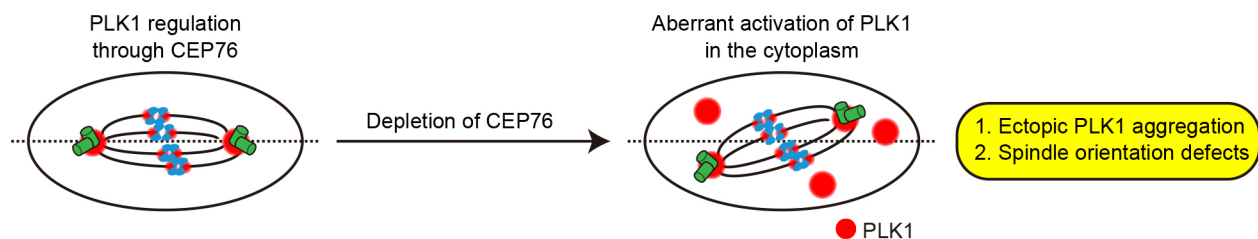

Fig. 8. A speculative model of CEP76-depletion phenotypes. A speculative model of CEP76-depletion phenotypes in mitotic human cells. CEP76 localizes at centrioles and suppresses the aberrant activation of PLK1. In the absence of CEP76, aberrantly activated PLK1 leads to mitotic defects, including the ectopic aggregation of PLK1 and spindle orientation defects.

induces defective spindle orientation (Hanafusa et al., 2015; Miyamoto et al., 2017; Sana et al., 2018; Yan et al., 2015). On the other hand, we propose the new notion that aberrant activation of PLK1 in CEP76-depleted cells causes similar spindle orientation defects. PLK1 phosphorylates nuclear mitotic apparatus protein 1 (NuMA1) and suppresses its excess cortical localization, which is needed for precise spindle orientation. We hypothesize that the aberrant activation of PLK1 impedes the recruitment of sufficient NuMA1 to the cortical region and induces spindle orientation defects. This scenario may explain mitotic spindle defects and the subsequent chromosome instability observed in some cancer cells that express PLK1 at high levels. Further investigations are warranted to verify this hypothesis.

Well-characterized functions of centrosomes during mitosis, microtubule nucleation and anchoring, are mainly achieved by the PCM, an amorphous mass of proteins surrounding centrioles (Nigg and Holland, 2018). However, apart from the accumulation of PCM, the functions of centrioles in mitosis are not fully understood. In this study, we revealed that CEP76, a centriolar protein, suppresses the aberrant activation of cytoplasmic PLK1 and following ectopic PLK1 aggregation during mitosis. Moreover, this PLK1 regulation was suggested to ensure proper spindle orientation. Therefore, our study sheds light on a function of centrioles in the regulation of mitotic PLK1, at least in part. Centrioles may act as a platform for the accumulation of various proteins (e.g. PLK1, CEP76) to efficiently regulate protein stability, activity and interactions.

CEP76 limits the re-duplication of centrioles during interphase in certain types of human cancer cells (Tsang et al., 2009). This function depends on the phosphorylation of CEP76 by CDK2 and subsequent activation of PLK1 (Barbelanne et al., 2016). Centriole amplification was also observed in our experiments using U2OS cells (Fig. S8B,C). In addition to the function of CEP76 in interphase, we identified the function of CEP76 in mitosis; it properly suppresses the aberrant activation and ectopic aggregation of PLK1. Collectively, the results of previous studies and the present investigation suggest that CEP76 is important for the regulation of PLK1 both in interphase and mitosis to maintain cell homeostasis throughout the cell cycle in various aspects, such as the suppression of centriole amplification and maintenance of spindle orientation.

Almost all experiments in this study were performed using HeLa cells, an immortal cell line derived from cervical cancer. In this study, HeLa cells exhibited drastic phenotypes upon depletion of CEP76 (Fig. S8D,H,I). However, the strength of the phenotypes appeared to be dependent on the type of cell examined (Fig. S8D–I). For example, PANC-1 cells, cancer cells isolated from a pancreatic carcinoma, likewise formed ectopic PLK1 aggregates upon depletion of CEP76 (Fig. S8E,H). Conversely, U2OS and RPE-1 cells did not show cytoplasmic aggregation of PLK1 upon depletion of CEP76 (Fig. S8F–H). In terms of spindle orientation, among the four cell lines tested, only HeLa cells exhibited severe defects (Fig. S8I). On the other hand, the centriole amplification phenotype upon depletion of CEP76 was observed in U2OS cells, but not in HeLa cells (Fig. S8A–C). Similar results were observed in previous studies of CEP76 function (Barbelanne et al., 2016; Tsang et al., 2009). The opposite correlation in the phenotypes is an interesting observation that warrants further investigation. Therefore, it is important to investigate the mechanisms through which the genetic backgrounds and other characteristics of cells influence the phenotypic strength in response to compromised CEP76 function.

It has been suggested that the expression level of PLK1 has a robust relationship with oncogenesis. Of note, PLK1 positively promotes cell cycle progression (Colicino and Hehnly, 2018). It has

been shown that the expression level of PLK1 is increased in various types of cancer cells, and its overexpression promotes the malignant transformation of a tumor (Fu and Wen, 2017; Takai et al., 2005). Therefore, specific inhibitors of PLK1 have been developed as anticancer drugs, and some are currently being investigated in clinical trials (Liu et al., 2017; Takai et al., 2005). However, results have revealed that PLK1 inhibitors exert limited anticancer activity. The reasons for these obstacles in drug development are currently unclear, and further understanding of the molecular properties of PLK1 is important to achieve a breakthrough in the future. Based on the findings of this study, it is conceivable that mutations affecting the expression or function of CEP76 might be associated with carcinogenesis. The regulation of PLK1 through the function of CEP76 and unidentified cofactors may be an attractive target for novel anticancer therapies. Therefore, further research is needed to delimitate the detailed molecular mechanisms.

MATERIALS AND METHODS
Cell culture and transfection
HeLa, U2OS, RPE-1, and HEK293T cells were obtained from the European Collection of Authenticated Cell Cultures (ECACC). These cell lines were authenticated by ECACC via short tandem repeat (STR) profiling. PANC-1 cells were obtained from RIKEN Bioresource Research Center (RIKEN BRC). This cell line was authenticated by RIKEN BRC via STR profiling. HEK GP2-293 cells were obtained from Clontech. This cell line was authenticated by Clontech via STR profiling. It was confirmed that the HeLa, U2OS and RPE-1 cells were not contaminated with mycoplasma using indirect DNA staining by Hoechst 33258 with indicator cells (Vero cells). The HEK293T, PANC-1 and HEK GP2-293 cells were confirmed as not being contaminated with mycoplasma by ECACC, RIKEN BRC or Clontech, respectively, before providing. The HeLa, U2OS, HEK293T and HEK GP2-293 cells were cultured in Dulbecco's modified Eagle's medium (DMEM; Nacalai Tesque, 08459-64), containing 10% fetal bovine serum (FBS), 100 U/ml penicillin and 100 μg/ml streptomycin, at 37°C in a 5% CO_2 atmosphere. The RPE-1 cells were cultured in DMEM/F-12 medium (Nacalai Tesque, 11581-15), containing 10% FBS, 100 U/ml penicillin and 100 μg/ml streptomycin, at 37°C in a 5% CO_2 atmosphere. The PANC-1 cells were cultured in RPMI 1640 medium (Nacalai Tesque, 30264-56), containing 10% FBS, 100 U/ml penicillin and 100 μg/ml streptomycin, at 37°C in a 5% CO_2 atmosphere.

Transfection of plasmid DNA and siRNA was performed using Lipofectamine 2000 and Lipofectamine RNAiMAX (Life Technologies), respectively, according to the manufacturer's instruction. Unless otherwise noted, the transfected cells were analyzed 48 h after transfection with siRNA and 24 h after transfection with DNA constructs.

Generation of stable cell lines
HeLa cells expressing PLK1 endogenously tagged with mCherry (HeLa EGFP–centrin-1 PLK1–mCherry) were generated using the CRISPR/Cas9 system, as previously described, with slight modifications (Natsume et al., 2016). GuideRNA oligos (PLK1_gRNA_F, 5′-CACCGGAGGCCTTGAG-ACGGTTGC-3′; and PLK1_gRNA_R, 5′-AAACGCAACCGTCTCAAG-GCCTCC-3′) were annealed and cloned into the *Bbs*I site of pX330-U6-Chimeric_BB-CBh-hSpCas9 (pX330-hSpCas9). The pX330-hSpCas9 plasmid was purchased from Addgene (#42230). To construct the donor plasmid for homology-directed repair, homology arms of the PLK1 locus (chr16:23689693–23690460) were amplified (pBS2_PLK1 C-ter_InsF, 5′-GGTATCGATAAGCTTCAGGCGCAGGAGAGAGCTGG-3′; and pB-S2_PLK1 C-ter_InsR, 5′-CGCTCTAGAACTAGTAAGACTGGCAGAG-GCTGGGC-3′) from the genomic DNA of HeLa cells and cloned into pBluescript using an Infusion Cloning Kit (Takara). A *BamH*I sequence and silent mutation to prevent re-cutting were generated in the middle of the homology arm domain. The mCherry cassette containing a hygromycin-resistance gene was introduced into the *BamH*I site in the middle of homology arms. The plasmids were introduced into HeLa cells stably expressing EGFP–centrin-1 (Tsuchiya et al., 2016) and then isolated by using the limited dilution method with hygromycin.

HeLa Tet-On 3G cells and HeLa Tet-On-PLK1 cells were generated using the retroviral Tet-On 3G inducible expression system (Clontech). HeLa Tet-On 3G cells were generated according to the manufacturer's protocol (Retro-X Tet-On 3G Inducible Expression System User Manual) and subjected to selection in medium containing blasticidin (10 µg/ml). To generate HeLa Tet-On-PLK1 cells, retroviral-mediated integration was used. The cDNA encoding full-length PLK1 was cloned into pRetro-TRE3G (Clontech) and co-transfected with the envelope vector pCMV-VSV-G (Addgene #8454) to HEK GP2-293 cells. The virus-containing medium was harvested and filtered using a 0.22 µm filter (Millipore). Pre-seeded HeLa Tet-On 3G cells were infected by the virus-containing medium which was supplemented with fresh medium, FBS and 4 µg/ml polybrene (Sigma) and subjected to selection in medium containing puromycin (2 µg/ml).

Expression of sgRNA to target CEP76
HeLa cells stably expressing Cas9 (HeLa-Cas9) have been previously described (Watanabe et al., 2019). The hSpCas9 sequences in the pX330-hSpCas9 (Addgene #42230) plasmid were substituted by PuroR coding sequences (pX330-PuroR). A single guide RNA (sgRNA) oligo targeting the CEP76 locus (sgCEP76; forward, 5′-CACCGATTGTGGATGCACA-CAGAGG-3′; reverse, 5′-AAACCCTCTGTGTGCATCCACAATC-3′) was cloned into the BbsI site of pX330-PuroR. The vector expressing sgCEP76 was introduced into HeLa-Cas9 cells using Lipofectamine 2000 and subjected to selection in medium containing puromycin (2 µg/ml).

Plasmid construction
The cDNA encoding full-length CEP76 isoform a (NCBI NP_079175.2) was amplified from a cDNA library of HeLa cells. The cDNA encoding full-length CEP192 was amplified from the pcDNA3-FLAG construct encoding full-length CEP192, which was kindly provided by Erich Nigg (University of Basel, Switzerland). The cDNA encoding full-length or fragmented PLK1 was amplified from the pRcCMV myc-Plk1 wt (Nigg RG6), which was purchased from Addgene (#41160). The CEP76 cDNA was subcloned into pCMV5-HA. The CEP192 and PLK1 cDNA were subcloned into pCMV5-FLAG. The pCMV5-HA vector and the pCMV5-FLAG vector were as used in previous research (Watanabe et al., 2019).

RNA interference
The following siRNAs were used: Silencer Select siRNA (Life Technologies) against CEP76 #1 (s36721), CEP76 #2 (s36723), CEP57 (s18694), CEP97 (s35887), CEP135 (s18587), CEP192 (s226819), CEP295 (s229742), SAS6 (s47487), PCNT (s10138), ODF2 (s9827), CPAP (s31622), STIL (s12863) and negative control (4390843). Custom siRNA (JBios) against ORF of CEP152 (5′-GCGGATCCAACTGGAAATCTA-3′).

Chemicals
The following chemicals were used in this study: centrinone (a PLK4 inhibitor; MedChemExpress, HY-18682) and BI 2536 (a PLK1 inhibitor; AdooQ, A10134).

Antibodies
The following primary antibodies were used in this study: rabbit polyclonal antibodies against PLK1 [Bethyl Laboratories, A300-251A; immunofluorescence (IF) 1:500, western blotting (WB) 1:1000], CEP192 (Bethyl Laboratories, A302-324A; IF 1:1000, WB 1:1000), α-tubulin (MBL, PM054, Lot 007; IF 1:500), CEP76 (Bethyl Laboratories, A302-326A; IF 1:200–1:500, WB 1:1000) and CP110 (Proteintech, 12780-1-AP; IF 1:500); mouse monoclonal antibodies against centrin (Merck Milipore, Clone 20H5, 04-1624; IF 1:1000), polyglutamylation modification (AdipoGen, AG-20B-0020-C100, Clone GT335; IF 1:1000), FLAG (Sigma, F1804-200UG, Clone M2; IF 1:1000, WB 1:1000), α-tubulin (Sigma, T5168, Clone B-5-1-2; IF 1:1000, WB 1:1000–1:5000), HSP90 (BD Biosciences, Lot 8198637, 610419; WB 1:2000), SAS6 (SantaCruz, sc-81431, Lot C0613; IF 1:500), PCNT (Abcam, ab28144, Lot GR305517-5; IF 1:500), NEDD1 (Abcam, ab57336, Lot GR266030-1; IF 1:500), and pT210-PLK1(Abcam, ab39068, Lot GR256220-27; IF 1:300); a rat monoclonal antibody against EB1 (Abcam, ab53358, Lot GR233220-24; IF 1:1000). Alexa Fluor 647-labeled

CEP152 (Bethyl Laboratories, A302-479A; IF 1:500) and Alexa Fluor 647-labeled CEP192 (Bethyl Laboratories, A302-324A; IF 1:500) were generated with Alexa Flour labeling kits (Life Technologies, A20186). The following secondary antibodies were used: Alexa Fluor 488 goat anti-mouse IgG (H+L; Molecular Probes, A-11001; IF 1:500), Alexa Fluor 555 goat anti-rabbit IgG (H+L; Molecular Probes, A-21428; IF 1:500), horseradish peroxidase-conjugated goat polyclonal antibodies against mouse IgG (Promega, W402B; WB 1:5000–1:10,000), and horseradish peroxidase-conjugated goat polyclonal antibodies against rabbit IgG (Promega, W401B; WB 1:5000–1:10,000). The primary antibodies against CEP76 or pT210-PLK1 were validated in Figs S4A,B, S7C,D. The other primary antibodies were used in previous studies (Chinen et al., 2020; Liccardi et al., 2019; Vacher et al., 2011; Watanabe et al., 2019; Yoshiba et al., 2019).

Immunostaining
For the immunofluorescence analyses, cells cultured on coverslips (Matsunami, No. 1) were fixed using −30°C methanol for 7 min and washed three times with phosphate-buffered saline (PBS). After that, using PBS with 0.05% Triton X-100 (PBS-X) for 5 min, the cells were permeabilized and blocked in 1% bovine serum albumin (BSA) in PBS-X for 30 min at room temperature. The cells were then incubated with primary antibodies for 8–24 h at 4°C, washed with PBS-X three times, and incubated with secondary antibodies and Hoechst 33258 solution (DOJINDO, NA134, 1:3000–1:5000) for 1–2 h at room temperature. The cells were washed three times with PBS-X and mounted onto glass slides (Matsunami, S0318).

Microscopy for immunofluorescence analysis
For all imaging except that shown in Fig. 4C and Fig. S3C,D, an Axioplan2 fluorescence microscope (Carl Zeiss) was used. For the imaging shown in Fig. S3C,D, a Leica TCS SP8 system equipped with a Leica HCX PL APO×63/1.4 oil CS2 objective and excitation wavelengths 405, 488, 561, and 647 nm was used. The pinhole was adjusted to 1.0 airy units. Scan speed was set to 200 Hz. For deconvolution, Huygens essential software (SVI; Scientific Volume Imaging) was used. For the imaging shown in Fig. 4C, a Zeiss 980 laser-scanning microscope with Airyscan2 equipped with a 63× Plan-Apochromat (1.4 NA) objective and excitation wavelengths 405, 488, 561, and 639 nm was used. Images were Airyscan processed using Zen software (Zeiss).

Maximum intensity z-projections for the representative images and sum of slices z-projections for the quantifications were generated using the FIJI distribution of the ImageJ (NIH) software. Optical slice numbers and step sizes of z-stacks are described in the figure legends.

Live-cell imaging
A Confocal Scanner Box, Cell Voyager CV1000 (Yokogawa Electric Corp.), equipped with a ×60 oil immersion objective lens and a stage incubator for a 35-mm dish was used for live-cell imaging. HeLa cells stably expressing EGFP–centrin-1 and PLK1 endogenously tagged with mCherry were cultured on 35-mm glass-bottom dishes (Greiner Bio-One, #627870) at 37°C in a 5% CO$_2$ atmosphere. Before imaging, cells were treated with siRNAs for 24 h. Images were taken using a back-illuminated EMCCD camera. After 24 h following transfection, the cells were visualized every 4 min over 24 h. The images were collected at 1.3 µm z steps. Maximum intensity z-projections were generated using the FIJI distribution of the ImageJ (NIH) software.

Immunoprecipitation
For preparation of human cell lysates for western blotting, HEK293T cells were collected 24 h after transfection, lysed on ice in lysis buffer [20 mM Tris-HCl pH 7.5, 50 mM NaCl, 1% Triton X-100, 5 mM EGTA, 1 mM DTT, 2 mM MgCl$_2$ and 1:1000 protease inhibitor cocktail (Nacalai Tesque, 25955-11)]. Insoluble material was removed after centrifugation at 20,800 *g* for 10 min. For immunoprecipitation of FLAG-tagged proteins, whole-cell lysates were incubated with FLAG antibody-conjugated M2 agarose gel (Merck Millipore, A2220) for 2 h at 4°C. The beads were washed at least three times with lysis buffer and resuspended in sodium dodecyl sulfate (SDS) sample buffer (Nacalai Tesque, 09499-14) for 5 min at 95°C.

Western blotting

Protein samples were subjected to SDS–PAGE on a 6–10% polyacrylamide gel then transferred onto Immobilon-P membrane (Merck Millipore, IPVH85R). The membrane was incubated in 2.5% skim milk in PBS containing 0.02% Tween (PBS-T) for 30 min at room temperature and washed three times. After that, the membrane was probed with the primary antibodies in 5% BSA in PBS-T for 8–12 h at 4°C, then washed three times. The membrane was then incubated with HRP-conjugated secondary antibodies in 2.5% skim milk in PBS-T for 1 h at room temperature and washed three times. The signals were detected using Amersham ECL Prime western blotting detection reagent (GE Healthcare, RPN2232), Amersham ECL Select western blotting detection reagent (GE Healthcare, RPN2235) or Chemi-Limi One Ultra (Nacalai Tesque, 11644-24), and a Chemi Doc XRC+ (BioRad).

Yeast two-hybrid analysis

Full-length CEP76 and PLK1 were cloned into the vectors pSM671 (bait) and pSM378 (prey), respectively, which were kindly provided by Satoru Mimura (Osaka University, Japan). Yeast strain L40, which was kindly provided by Masato Kanemaki (National Institute of Genetics, Mishima, Japan), was grown in YPD medium and transformed with the indicated vectors. Positive colonies were grown on SD plates lacking leucine and tryptophan in the presence of histidine at 30°C. After a few days, cells were spotted on plates containing 200 mM 3-Amino-1,2,4-triazole (Merck) without leucine, tryptophan and histidine. The plates were incubated at 30°C for a few days.

Statistical analysis

Statistical analyses were performed using the GraphPad Prism 7 software or Microsoft Office Excel. Statistical methods were not used to predetermine sample sizes. No data were excluded from the analyses. Reproducibility was confirmed in all the experimental results. We assessed cells from several fields of view for each experiment. The fields of view were randomly chosen. Once a field of view was determined, we counted all cells that matched the criteria within the field. The investigators were not blinded to the sample ID during experiments and outcome assessments. For significance tests, except those in Figs S1E,F and S8C, we used non-parametric methods (Mann–Whitney U-test or Kruskal–Wallis test). In Figs S1E,F and S8C, we used unpaired t-tests. Details are described in the figure legends.

References

Barbelanne, M., Chiu, A., Qian, J. and Tsang, W. Y. (2016). Opposing post-translational modifications regulate Cep76 function to suppress centriole amplification. *Oncogene* **35**, 5377-5387. doi:10.1038/onc.2016.74

Barr, F. A., Silljé, H. H. W. and Nigg, E. A. (2004). Polo-like kinases and the orchestration of cell division. *Nat. Rev. Mol. Cell Biol.* **5**, 429-441. doi:10.1038/nrm1401

Bruinsma, W., Macůrek, L., Freire, R., Lindqvist, A. and Medema, R. H. (2014). Bora and Aurora-A continue to activate Plk1 in mitosis. *J. Cell Sci.* **127**, 801-811. doi:10.1242/jcs.137216

Chinen, T., Yamamoto, S., Takeda, Y., Watanabe, K., Kuroki, K., Hashimoto, K., Takao, D. and Kitagawa, D. (2020). NuMA assemblies organize microtubule asters to establish spindle bipolarity in acentrosomal human cells. *EMBO J.* **39**, 1-18. doi:10.15252/embj.2019102378

Cizmecioglu, O., Arnold, M., Bahtz, R., Settele, F., Ehret, L., Haselmann-Weiß, U., Antony, C. and Hoffmann, I. (2010). Cep152 acts as a scaffold for recruitment of Plk4 and CPAP to the centrosome. *J. Cell Biol.* **191**, 731-739. doi:10.1083/jcb.201007107

Colicino, E. G. and Hehnly, H. (2018). Regulating a key mitotic regulator, polo–like kinase 1 (PLK1). *Cytoskeleton* **75**, 481-494. doi:10.1002/cm.21504

Conduit, P. T., Wainman, A. and Raff, J. W. (2015). Centrosome function and assembly in animal cells. *Nat. Rev. Mol. Cell Biol.* **16**, 611-624. doi:10.1038/nrm4062

de Cárcer, G., Manning, G. and Malumbres, M. (2011). From Plk1 to Plk5. *Cell Cycle* **10**, 2255-2262. doi:10.4161/cc.10.14.16494

Dictenberg, J. B., Zimmerman, W., Sparks, C. A., Young, A., Vidair, C., Zheng, Y., Carrington, W., Fay, F. S. and Doxsey, S. J. (1998). Pericentrin and γ-tubulin form a protein complex and are organized into a novel lattice at the centrosome. *J. Cell Biol.* **141**, 163-174. doi:10.1083/jcb.141.1.163

Doxsey, S. J., Stein, P., Evans, L., Calarco, P. D. and Kirschner, M. (1994). Pericentrin, a highly conserved centrosome protein involved in microtubule organization. *Cell* **76**, 639-650. doi:10.1016/0092-8674(94)90504-5

Dzhindzhev, N. S., Yu, Q. D., Weiskopf, K., Tzolovsky, G., Cunha-Ferreira, I., Riparbelli, M., Rodrigues-Martins, A., Bettencourt-Dias, M., Callaini, G. and Glover, D. M. (2010). Asterless is a scaffold for the onset of centriole assembly. *Nature* **467**, 714-718. doi:10.1038/nature09445

Fu, Z. and Wen, D. (2017). The emerging role of polo-like kinase 1 in epithelial-mesenchymal transition and tumor metastasis. *Cancers* **9**, 131. doi:10.3390/cancers9100131

Golsteyn, R. M. (1995). Cell cycle regulation of the activity and subcellular localization of Plk1, a human protein kinase implicated in mitotic spindle function. *J. Cell Biol.* **129**, 1617-1628. doi:10.1083/jcb.129.6.1617

Gomez-Ferreria, M. A., Rath, U., Buster, D. W., Chanda, S. K., Caldwell, J. S., Rines, D. R. and Sharp, D. J. (2007). Human Cep192 is required for mitotic centrosome and spindle assembly. *Curr. Biol.* **17**, 1960-1966. doi:10.1016/j.cub.2007.10.019

Gönczy, P. (2015). Centrosomes and cancer: revisiting a long-standing relationship. *Nat. Rev. Cancer* **15**, 639-652. doi:10.1038/nrc3995

Habedanck, R., Stierhof, Y.-D., Wilkinson, C. J. and Nigg, E. A. (2005). The Polo kinase Plk4 functions in centriole duplication. *Nat. Cell Biol.* **7**, 1140-1146. doi:10.1038/ncb1320

Hanafusa, H., Kedashiro, S., Tezuka, M., Funatsu, M., Usami, S., Toyoshima, F. and Matsumoto, K. (2015). PLK1-dependent activation of LRRK1 regulates spindle orientation by phosphorylating CDK5RAP2. *Nat. Cell Biol.* **17**, 1024-1035. doi:10.1038/ncb3204

Hatch, E. M., Kulukian, A., Holland, A. J., Cleveland, D. W. and Stearns, T. (2010). Cep152 interacts with Plk4 and is required for centriole duplication. *J. Cell Biol.* **191**, 721-729. doi:10.1083/jcb.201006049

Hu, C.-K., Özlü, N., Coughlin, M., Steen, J. J. and Mitchison, T. J. (2012). Plk1 negatively regulates PRC1 to prevent premature midzone formation before cytokinesis. *Mol. Biol. Cell* **23**, 2702-2711. doi:10.1091/mbc.e12-01-0058

Ishikawa, H., Kubo, A., Tsukita, S. and Tsukita, S. (2005). Odf2-deficient mother centrioles lack distal/subdistal appendages and the ability to generate primary cilia. *Nat. Cell Biol.* **7**, 517-524. doi:10.1038/ncb1251

Joukov, V., De Nicolo, A., Rodriguez, A., Walter, J. C. and Livingston, D. M. (2010). Centrosomal protein of 192 kDa (Cep192) promotes centrosome-driven spindle assembly by engaging in organelle-specific Aurora A activation. *Proc. Natl. Acad. Sci. USA* **107**, 21022-21027. doi:10.1073/pnas.1014664107

Joukov, V., Walter, J. C. and De Nicolo, A. (2014). The Cep192-organized aurora A-Plk1 cascade is essential for centrosome cycle and bipolar spindle assembly. *Mol. Cell* **55**, 578-591. doi:10.1016/j.molcel.2014.06.016

Kang, Y. H., Park, J.-E., Yu, L.-R., Soung, N.-K., Yun, S.-M., Bang, J. K., Seong, Y.-S., Yu, H., Garfield, S., Veenstra, T. D. et al. (2006). Self-regulated Plk1 recruitment to kinetochores by the Plk1-PBIP1 interaction is critical for proper chromosome segregation. *Mol. Cell* **24**, 409-422. doi:10.1016/j.molcel.2006.10.016

Kim, J., Kim, J. and Rhee, K. (2019). PCNT is critical for the association and conversion of centrioles to centrosomes during mitosis. *J. Cell Sci.* **132**, jcs225789. doi:10.1242/jcs.225789

Kitagawa, D., Vakonakis, I., Olieric, N., Hilbert, M., Keller, D., Olieric, V., Bortfeld, M., Erat, M. C., Flückiger, I., Gönczy, P. et al. (2011). Structural basis of the 9-fold symmetry of centrioles. *Cell* **144**, 364-375. doi:10.1016/j.cell.2011.01.008

Kleylein-Sohn, J., Westendorf, J., Le Clech, M., Habedanck, R., Stierhof, Y.-D. and Nigg, E. A. (2007). Plk4-induced centriole biogenesis in human cells. *Dev. Cell* **13**, 190-202. doi:10.1016/j.devcel.2007.07.002

Knoblich, J. A. (2010). Asymmetric cell division: recent developments and their implications for tumour biology. *Nat. Rev. Mol. Cell Biol.* **11**, 849-860. doi:10.1038/nrm3010

Kumar, S., Sharma, A. R., Sharma, G., Chakraborty, C. and Kim, J. (2016). PLK-1: Angel or devil for cell cycle progression. *Biochim. Biophys. Acta Rev. Cancer* **1865**, 190-203. doi:10.1016/j.bbcan.2016.02.003

Lee, K. and Rhee, K. (2011). PLK1 phosphorylation of pericentrin initiates centrosome maturation at the onset of mitosis. *J. Cell Biol.* **195**, 1093-1101. doi:10.1083/jcb.201106093

Lee, K. S., Park, J.-E., Kang, Y. H., Kim, T.-S. and Bang, J. K. (2014). Mechanisms underlying Plk1 polo-box domain-mediated biological processes and their physiological significance. *Mol. Cells* **37**, 286-294. doi:10.14348/molcells.2014.0002

Leidel, S., Delattre, M., Cerutti, L., Baumer, K. and Gönczy, P. (2005). SAS-6 defines a protein family required for centrosome duplication in C. elegans and in human cells. *Nat. Cell Biol.* **7**, 115-125. doi:10.1038/ncb1220

Liccardi, G., Ramos Garcia, L., Tenev, T., Annibaldi, A., Legrand, A. J., Robertson, D., Feltham, R., Anderton, H., Darding, M., Peltzer, N. et al. (2019). RIPK1 and caspase-8 ensure chromosome stability independently of their role in cell death and inflammation. *Mol. Cell* **73**, 413-428. doi:10.1016/j.molcel.2018.11.010

Lin, Y.-C., Chang, C.-W., Hsu, W.-B., Tang, C.-J. C., Lin, Y.-N., Chou, E.-J., Wu, C.-T. and Tang, T. K. (2013). Human microcephaly protein CEP135 binds to hSAS-6 and CPAP, and is required for centriole assembly. *EMBO J.* **32**, 1141-1154. doi:10.1038/emboj.2013.56

Liu, Z., Sun, Q. and Wang, X. (2017). PLK1, A potential target for cancer therapy. *Transl. Oncol.* **10**, 22-32. doi:10.1016/j.tranon.2016.10.003

Llamazares, S., Moreira, A., Tavares, A., Girdham, C., Spruce, B. A., Gonzalez, C., Karess, R. E., Glover, D. M. and Sunkel, C. E. (1991). polo encodes a protein kinase homolog required for mitosis in Drosophila. *Genes Dev.* **5**, 2153-2165. doi:10.1101/gad.5.12a.2153

Lu, M. S. and Johnston, C. A. (2013). Molecular pathways regulating mitotic spindle orientation in animal cells. *Development* **140**, 1843-1856. doi:10.1242/dev.087627

Miyamoto, T., Akutsu, S. N., Fukumitsu, A., Morino, H., Masatsuna, Y., Hosoba, K., Kawakami, H., Yamamoto, T., Shimizu, K., Ohashi, H. et al. (2017). PLK1-mediated phosphorylation of WDR62/MCPH2 ensures proper mitotic spindle orientation. *Hum. Mol. Genet.* **26**, 4429-4440. doi:10.1093/hmg/ddx330

Mukhopadhyay, D. and Dasso, M. (2010). The fate of metaphase kinetochores is weighed in the balance of SUMOylation during S phase. *Cell Cycle* **9**, 3214-3221. doi:10.4161/cc.9.16.12619

Mulvihill, D. P., Petersen, J., Ohkura, H., Glover, D. M. and Hagan, I. M. (1999). Plo1 Kinase recruitment to the spindle pole body and its role in cell division in Schizosaccharomyces pombe. *Mol. Biol. Cell* **10**, 2771-2785. doi:10.1091/mbc.10.8.2771

Natsume, T., Kiyomitsu, T., Saga, Y. and Kanemaki, M. T. (2016). Rapid protein depletion in human cells by auxin-inducible degron tagging with short homology donors. *Cell Rep.* **15**, 210-218. doi:10.1016/j.celrep.2016.03.001

Nigg, E. A. and Holland, A. J. (2018). Once and only once: mechanisms of centriole duplication and their deregulation in disease. *Nat. Rev. Mol. Cell Biol.* **19**, 297-312. doi:10.1038/nrm.2017.127

Nigg, E. A. and Raff, J. W. (2009). Centrioles, centrosomes, and cilia in health and disease. *Cell* **139**, 663-678. doi:10.1016/j.cell.2009.10.036

Sana, S., Keshri, R., Rajeevan, A., Kapoor, S. and Kotak, S. (2018). Plk1 regulates spindle orientation by phosphorylating NuMA in human cells. *Life Sci. Alliance* **1**, 1-14. doi:10.26508/lsa.201800223

Schmidt, T. I., Kleylein-Sohn, J., Westendorf, J., Le Clech, M., Lavoie, S. B., Stierhof, Y.-D. and Nigg, E. A. (2009). Control of centriole length by CPAP and CP110. *Curr. Biol.* **19**, 1005-1011. doi:10.1016/j.cub.2009.05.016

Schmit, T. L., Nihal, M., Ndiaye, M., Setaluri, V., Spiegelman, V. S. and Ahmad, N. (2012). Numb regulates stability and localization of the mitotic kinase PLK1 and is required for transit through mitosis. *Cancer Res.* **72**, 3864-3872. doi:10.1158/0008-5472.CAN-12-0714

Schmucker, S. and Sumara, I. (2014). Molecular dynamics of PLK1 during mitosis. *Mol. Cell. Oncol.* **1**, e954507. doi:10.1080/23723548.2014.954507

Siller, K. H. and Doe, C. Q. (2009). Spindle orientation during asymmetric cell division. *Nat. Cell Biol.* **11**, 365-374. doi:10.1038/ncb0409-365

Steegmaier, M., Hoffmann, M., Baum, A., Lénárt, P., Petronczki, M., Krššák, M., Gürtler, U., Garin-Chesa, P., Lieb, S., Quant, J. et al. (2007). BI 2536, a potent and selective inhibitor of polo-like kinase 1, inhibits tumor growth in vivo. *Curr. Biol.* **17**, 316-322. doi:10.1016/j.cub.2006.12.037

Stevens, N. R., Dobbelaere, J., Brunk, K., Franz, A. and Raff, J. W. (2010). Drosophila Ana2 is a conserved centriole duplication factor. *J. Cell Biol.* **188**, 313-323. doi:10.1083/jcb.200910016

Sunkel, C. E. and Glover, D. M. (1988). polo, a mitotic mutant of Drosophila displaying abnormal spindle poles. *J. Cell Sci.* **89**, 25-38.

Takai, N., Hamanaka, R., Yoshimatsu, J. and Miyakawa, I. (2005). Polo-like kinases (Plks) and cancer. *Oncogene* **24**, 287-291. doi:10.1038/sj.onc.1208272

Tang, C.-J. C., Fu, R.-H., Wu, K.-S., Hsu, W.-B. and Tang, T. K. (2009). CPAP is a cell-cycle regulated protein that controls centriole length. *Nat. Cell Biol.* **11**, 825-831. doi:10.1038/ncb1889

Tsang, W. Y., Spektor, A., Vijayakumar, S., Bista, B. R., Li, J., Sanchez, I., Duensing, S. and Dynlacht, B. D. (2009). Cep76, a centrosomal protein that specifically restrains centriole reduplication. *Dev. Cell* **16**, 649-660. doi:10.1016/j.devcel.2009.03.004

Tsou, M.-F. B. and Stearns, T. (2006). Mechanism limiting centrosome duplication to once per cell cycle. *Nature* **442**, 947-951. doi:10.1038/nature04985

Tsou, M.-F. B., Wang, W.-J., George, K. A., Uryu, K., Stearns, T. and Jallepalli, P. V. (2009). Polo kinase and separase regulate the mitotic licensing of centriole duplication in human cells. *Dev. Cell* **17**, 344-354. doi:10.1016/j.devcel.2009.07.015

Tsuchiya, Y., Yoshiba, S., Gupta, A., Watanabe, K. and Kitagawa, D. (2016). Cep295 is a conserved scaffold protein required for generation of a bona fide mother centriole. *Nat. Commun.* **7**, 12567. doi:10.1038/ncomms12567

Tsvetkov, L. and Stern, D. F. (2005). Phosphorylation of Plk1 at S137 and T210 is Inhibited in Response to DNA Damage. *Cell Cycle* **4**, 166-171. doi:10.4161/cc.4.1.1348

Vacher, H., Yang, J. W., Cerda, O., Autillo-Touati, A., Dargent, B. and Trimmer, J. S. (2011). Cdk-mediated phosphorylation of the Kvβ2 auxiliary subunit regulates Kv1 channel axonal targeting. *J. Cell Biol.* **192**, 813-824. doi:10.1083/jcb.201007113

Vidwans, S. J., Wong, M. L. and O′Farrell, P. H. (1999). Mitotic regulators govern progress through steps in the centrosome duplication cycle. *J. Cell Biol.* **147**, 1371-1378. doi:10.1083/jcb.147.7.1371

Watanabe, K., Takao, D., Ito, K. K., Takahashi, M. and Kitagawa, D. (2019). The Cep57-pericentrin module organizes PCM expansion and centriole engagement. *Nat. Commun.* **10**, 931. doi:10.1038/s41467-019-08862-2

Wong, Y. L., Anzola, J. V., Davis, R. L., Yoon, M., Motamedi, A., Kroll, A., Seo, C. P., Hsia, J. E., Kim, S. K., Mitchell, J. W. et al. (2015). Reversible centriole depletion with an inhibitor of Polo-like kinase 4. *Science* **348**, 1155-1160. doi:10.1126/science.aaa5111

Yan, M., Chu, L., Qin, B., Wang, Z., Liu, X., Jin, C., Zhang, G., Gomez, M., Hergovich, A., Chen, Z. et al. (2015). Regulation of NDR1 activity by PLK1 ensures proper spindle orientation in mitosis. *Sci. Rep.* **5**, 1-14. doi:10.1038/srep10449

Yoshiba, S., Tsuchiya, Y., Ohta, M., Gupta, A., Shiratsuchi, G., Nozaki, Y., Ashikawa, T., Fujiwara, T., Natsume, T., Kanemaki, M. T. et al. (2019). HsSAS-6-dependent cartwheel assembly ensures stabilization of centriole intermediates. *J. Cell Sci.* **132**, jcs217521. doi:10.1242/jcs.217521

Zhao, W., Liu, J., Zhang, X. and Deng, L.-W. (2016). MLL5 maintains spindle bipolarity by preventing aberrant cytosolic aggregation of PLK1. *J. Cell Biol.* **212**, 829-843. doi:10.1083/jcb.201501021

Zhu, F., Lawo, S., Bird, A., Pinchev, D., Ralph, A., Richter, C., Müller-Reichert, T., Kittler, R., Hyman, A. A. and Pelletier, L. (2008). The mammalian SPD-2 ortholog Cep192 regulates centrosome biogenesis. *Curr. Biol.* **18**, 136-141. doi:10.1016/j.cub.2007.12.055
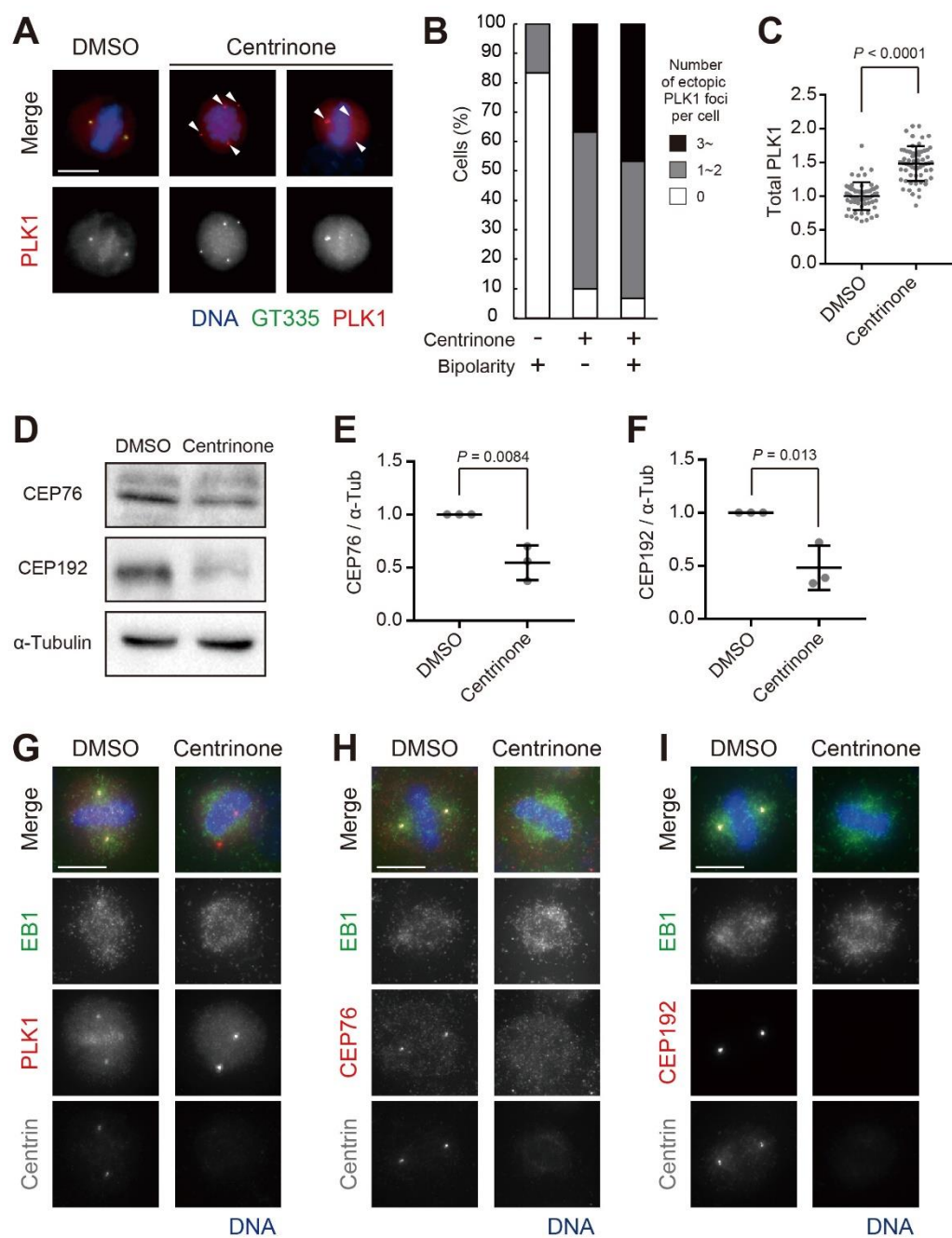
Supplementary Figure 1, Takeda.

Figure S1. Ectopic aggregation of PLK1 in the cytoplasm upon removal of centrosomes.

(A, B) HeLa cells were treated with dimethyl sulfoxide (DMSO; negative control; 0.1%) or centrinone (a PLK4 inhibitor; 100 nM), and immunostained with antibodies against polyglutamylation modification (GT335; green) and PLK1 (red). (A) Representative images of the cells treated with DMSO or centrinone. Arrowheads indicate the ectopic aggregates of PLK1. Z-projections (maximum intensity) of 21 sections, every 0.5 μm. Scale bar, 10 μm. (B) The cells in each group were categorized into three patterns according to the number of ectopic aggregates of PLK1 per cell. $N = 30$ cells. In the centrinone-treated cells, those without centrosomes (GT335 foci) were selected and divided into two groups according to the mitotic spindle structures, monopolar or bipolar. (C) The total amount of PLK1 signal in a mitotic cell was quantified (Z-projections [sum of slices] of 31 sections, every 1.0 μm). In this quantification, the cells selected in Fig. 1B were used. Line and error bars denote the mean intensity ± s.d. and the Mann–Whitney U test (two-tailed) was used to obtain P values. $N = 60$ cells from two independent experiments ($N = 30$ per experiment). (D–F) Whole-cell lysates from HeLa cells treated with DMSO (0.1%) or centrinone (100 nM) were blotted and examined using antibodies against CEP76, CEP192, and α-Tubulin. (D) Representative images of the bands detected by western blotting. (E) Quantification of CEP76 intensity normalized by that of α-Tubulin. Line and error bars denote the mean intensity ± s.d. and the unpaired t test (two-tailed) was used to obtain P values. $N = 3$ independent experiments. (F) Quantification of CEP192 intensity normalized by that of α-Tubulin. Line and error bars denote the mean intensity ± s.d. and the unpaired t test (two-tailed) was used to obtain P values. $N = 3$ independent experiments. (G) HeLa cells were treated with DMSO (0.1%) or centrinone (100 nM) and, immunostained with antibodies against EB1 (green), PLK1 (red), and

Centrin (gray). Representative images of the cells treated with DMSO or centrinone. (H) HeLa cells were treated with DMSO (0.1%) or centrinone (100 nM) and, immnostained with antibodies against EB1 (green), CEP76 (red), and Centrin (gray). Representative image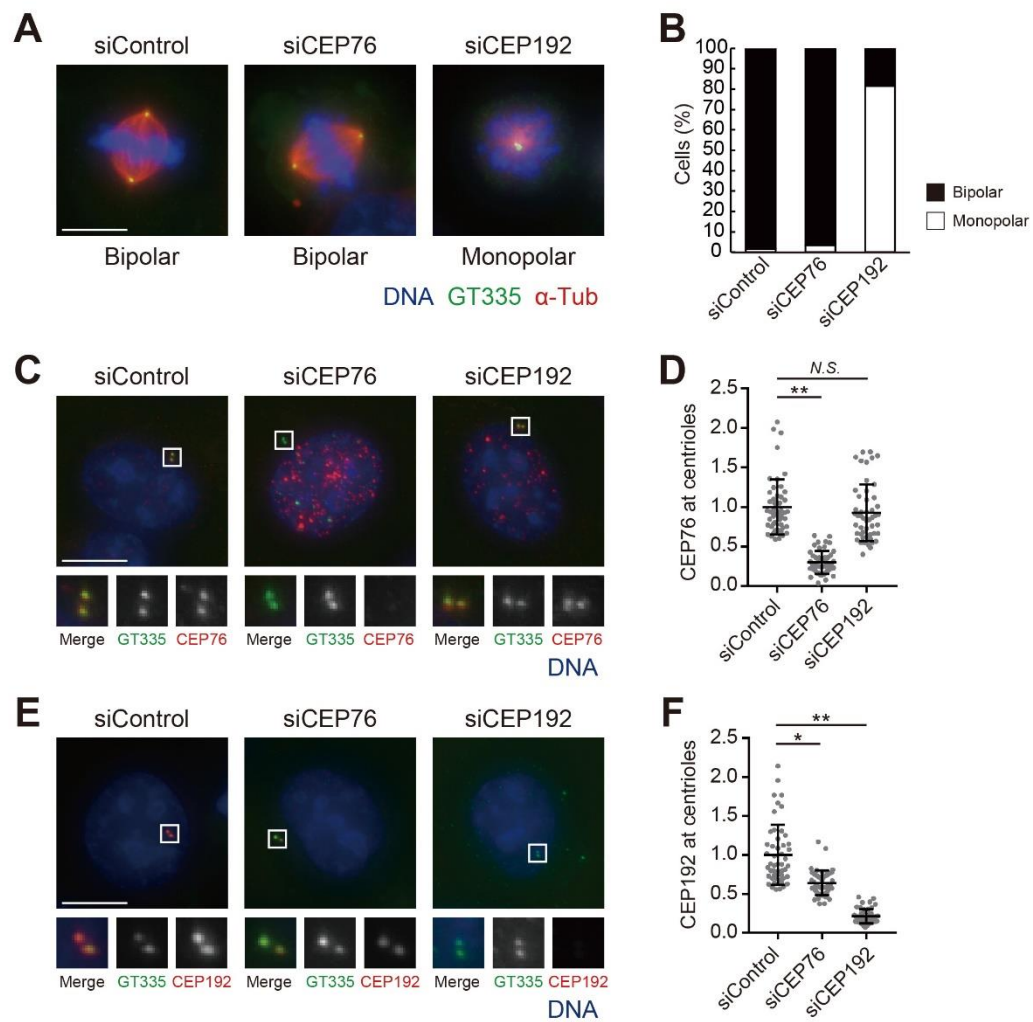s of the cells treated with DMSO or centrinone. (I) HeLa cells were treated with DMSO (0.1%) or centrinone (100 nM), and immnostained with antibodies against EB1 (green), CEP192 (red), and Centrin (gray). Representative images of the cells treated with DMSO or centrinone.

Supplementary Figure 2, Takeda et al.

Figure S2. Comparison of phenotypes of CEP76 and CEP192-depletion.

(A, B) HeLa cells were treated with siControl, siCEP76, or siCEP192, and immunostained with antibodies against GT335 (green) and α-Tubulin (red). (A) Representative images of the cells treated with siControl, siCEP76, or siCEP192. Z-projections (maximum intensity) of 21 sections, every 0.5 μm. Scale bar, 10 μm. (B) The cells in each group were categorized into two patterns according to the mitotic spindle structures, monopolar or bipolar. $N = 60$ cells from two independent experiments ($N = 30$ per experiment). (C, D) HeLa cells were treated with siControl, siCEP76, or siCEP192, and immunostained with antibodies against GT335 (green) and CEP76 (red). (C) Representative images of the interphase cells treated with siControl, siCEP76, or siCEP192. Z-projections (maximum intensity) of 21 sections, every 0.5 μm. Scale bar, 10 μm. (D) Quantification of CEP76 intensity at centrioles (GT335 foci) in the cells in each group. Line and error bars denote the mean intensity ± s.d. and the Kruskal–Wallis test was used to obtain P values. $N = 50$ centrosomes. $**P < 0.0001$. (E, F) HeLa cells were treated with siControl, siCEP76, or siCEP192, and immunostained with antibodies against GT335 (green) and CEP192 (red). (E) Representative images of the interphase cells treated with siControl, siCEP76, or siCEP192. Z-projections (maximum intensity) of 21 sections, every 0.5 μm. Scale bar, 10 μm. (F) Quantification of CEP192 intensity at centrioles (GT335 foci) in the cells in each group. Line and error bars denote the mean intensity ± s.d. and the Kruskal–Wallis test was used to obtain P values. $N = 50$ centrosomes. $**P < 0.0001$, $*P < 0.05$.
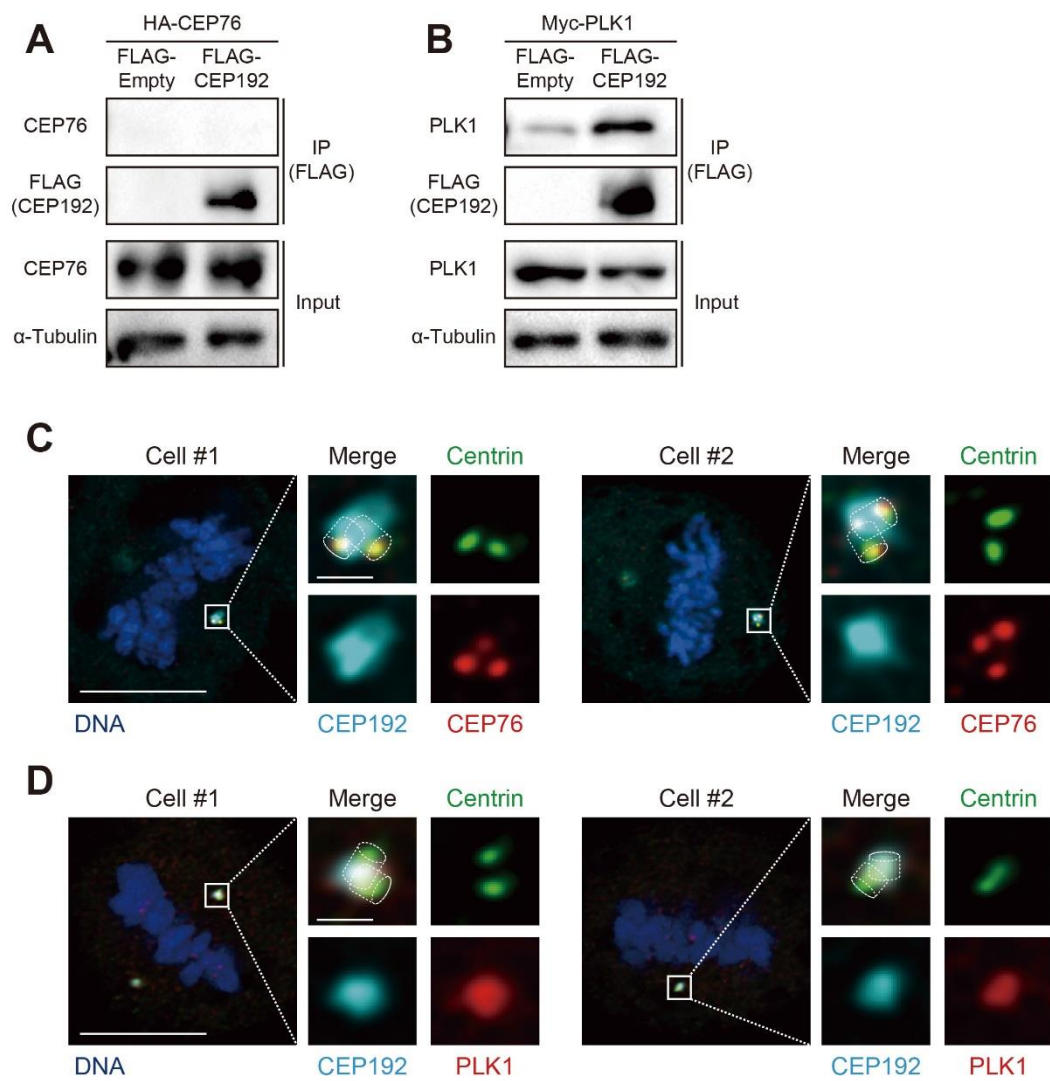
Supplementary Figure 3, Takeda et al.

Figure S3. Physical interaction and localization of CEP76, CEP192, and PLK1.

(A) HEK293T cells co-expressing FLAG-Empty (negative control) or FLAG-CEP192 and HA-CEP76 were immunoprecipitated with an antibody against FLAG-tag. The samples were blotted and examined using antibodies against CEP76, FLAG-tag, or α-Tubulin. (B) HEK293T cells co-expressing FLAG-Empty (negative control) or FLAG-CEP192 and Myc-PLK1 were immunoprecipitated with an antibody against FLAG-tag. The samples were blotted and examined using antibodies against PLK1, FLAG-tag, or α-Tubulin. (C) HeLa cells were immunostained with antibodies against Centrin (green), CEP76 (red), and CEP192 (cyan). Representative images of the cells. Single slice. Scale bar, 10 μm and 1 μm. (D) HeLa cells were immunostained with antibodies against Centrin (green), PLK1 (red), and CEP192 (cyan). Representative images of the cells. Single slice. Scale bar, 10 μm and 1 μm.
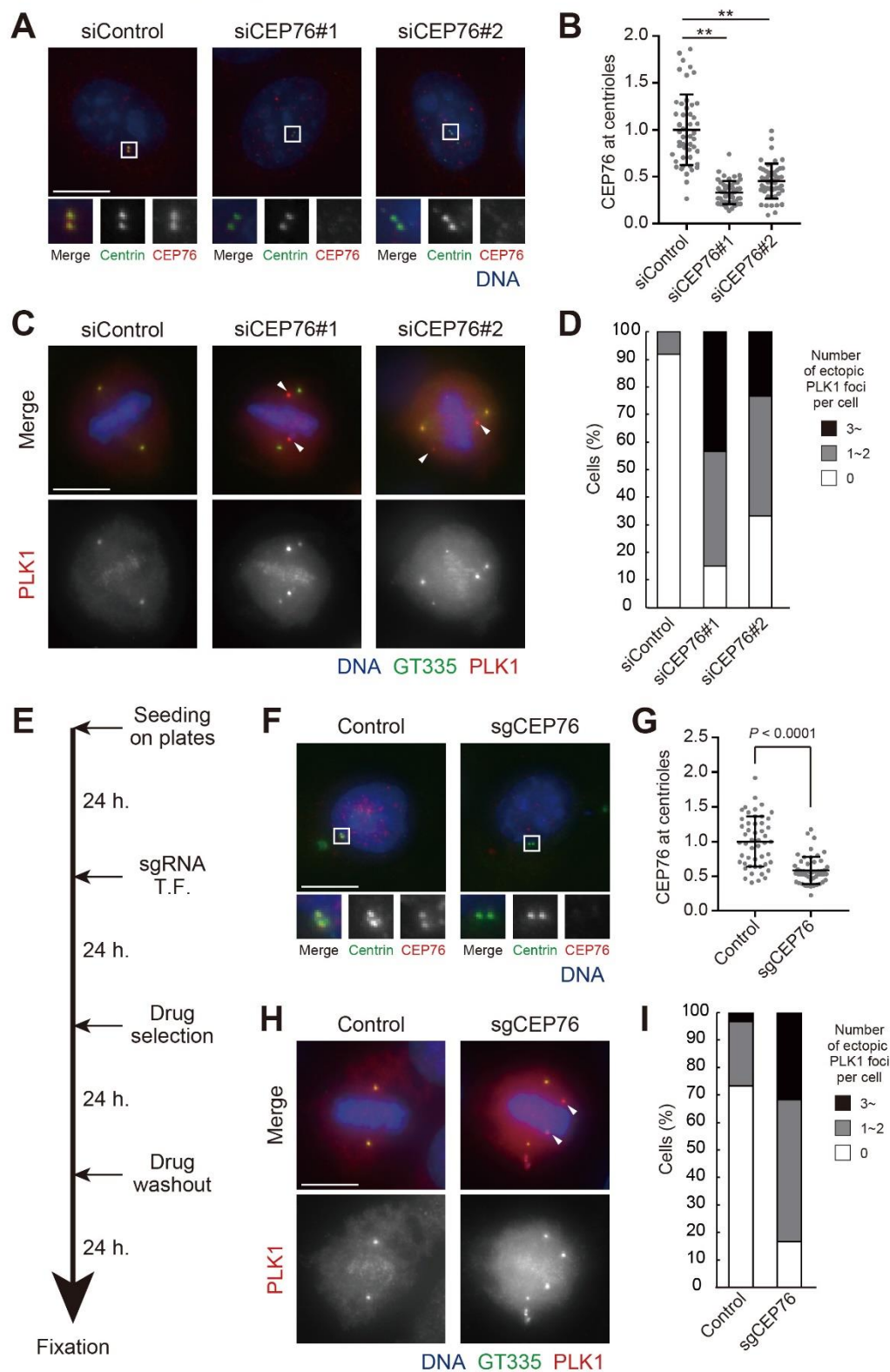
Supplementary Figure 4, Takeda.

Figure S4. Confirmation of the phenotype induced by CEP76-depletion.

(A, B) HeLa cells were treated with siControl, siCEP76#1, or siCEP76#2, and immunostained with antibodies against Centrin (green) and CEP76 (red). (A) Representative images of the cells treated with siControl, siCEP76#1, or siCEP76#2. Z-projections (maximum intensity) of 17 sections, every 0.25 μm. Scale bar, 10 μm. (B) Quantification of CEP76 intensity at centrioles (Centrin foci) in the cells in each group. Line and error bars denote the mean intensity ± s.d. and the Kruskal–Wallis test was used to obtain *P* values. $N = 50$ centrioles. **P < 0.0001. (C, D) HeLa cells were treated with siControl, siCEP76#1, or siCEP76#2, and immunostained with antibodies against GT335 (green) and PLK1 (red). (C) Representative images of the cells treated with siControl, siCEP76#1, or siCEP76#2. Arrowheads indicate the ectopic aggregates of PLK1. Z-projections (maximum intensity) of 21 sections, every 0.5 μm. Scale bar, 10 μm. (D) The cells in each group were categorized into three patterns according to the number of ectopic aggregates of PLK1 per cell. $N = 60$ cells from two independent experiments ($N = 30$ per experiment). (E) A schematic illustration showing the experimental conditions. HeLa cells stably expressing Cas9 (HeLa-Cas9 cells) were treated with sgRNA and selected by puromycin (2 μg/ml), and the puromycin was removed. (F, G) HeLa-Cas9 cells were treated with control sgRNA (Control) or sgRNA targeting a sequence in CEP76 (sgCEP76), and immunostained with antibodies against Centrin (green) and CEP76 (red). (F) Representative images of the cells treated with control sgRNA or sgCEP76. Z-projections (maximum intensity) of 21 sections, every 0.25 μm. Scale bar, 10 μm. (G) Quantification of CEP76 intensity at centrioles (Centrin foci) of the cells in each group. Line and error bars denote the mean intensity ± s.d. and the Mann–Whitney *U* test (two-tailed) was used to obtain *P* values. $N = 50$ centrioles. (H, I) HeLa-Cas9 cells were treated with control sgRNA (Control) or sgCEP76, and immunostained with antibodies against GT335 (green) and

PLK1 (red). (H) Representative images of the cells treated with control sgRNA or sgCEP76. Arrowheads indicate the ectopic aggregates of PLK1. Z-projections (maximum intensity) of 21 sections, every 0.5 μm. Scale bar, 10 μm. (I) The cells in each group were categorized into three patterns according to the number of ectopic aggregates of PLK1 per cell. $N = 60$ cells from two independent experiments ($N = 30$ per experiment).
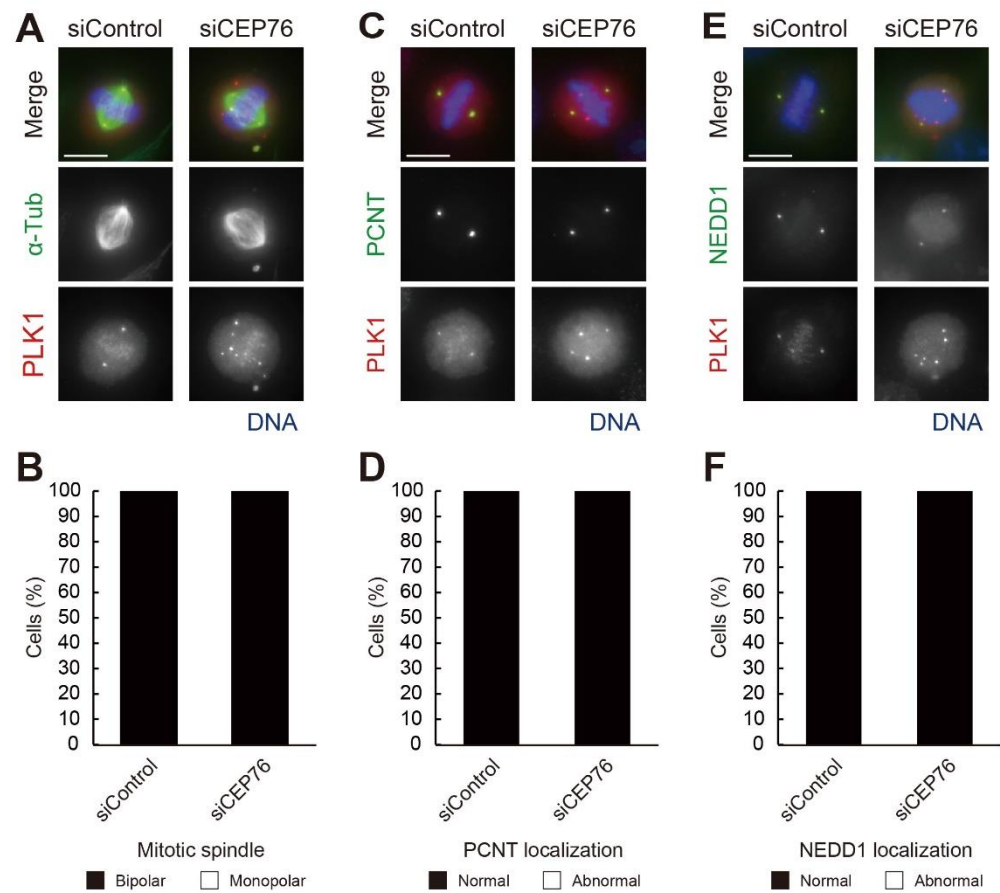
Supplementary Figure 5, Takeda.

Figure S5. The effect of CEP76-depletion on the mitotic spindle structures and the localization of PCM components.

(A, B) HeLa cells were treated with siControl or siCEP76, and immunostained with antibodies against α-Tubulin (green) and PLK1 (red). (A) Representative images of the cells treated with siControl or siCEP76. Z-projections (maximum intensity) of 21 sections, every 0.5 μm. Scale bar, 10 μm. (B) The cells in each group were categorized into two patterns according to the mitotic spindle structures, monopolar or bipolar. $N = 50$ cells. (C, D) HeLa cells were treated with siControl or siCEP76, and immunostained with antibodies against PCNT (green) and PLK1 (red). (C) Representative images of the cells treated with siControl or siCEP76. Z-projections (maximum intensity) of 21 sections, every 0.5 μm. Scale bar, 10 μm. (D) The cells in each group were categorized into two patterns according to the PCNT localization, normal (only two foci at spindle poles) or abnormal. $N = 50$ centrioles. (E, F) HeLa cells were treated with siControl or siCEP76, and immunostained with antibodies against NEDD1 (green) and PLK1 (red). (E) Representative images of the cells treated with siControl or siCEP76. Z-projections (maximum intensity) of 21 sections, every 0.5 μm. Scale bar, 10 μm. (F) The cells in each group were categorized into two patterns according to the NEDD1 localization, normal (only two foci at spindle poles) or abnormal. $N = 50$ centrioles.
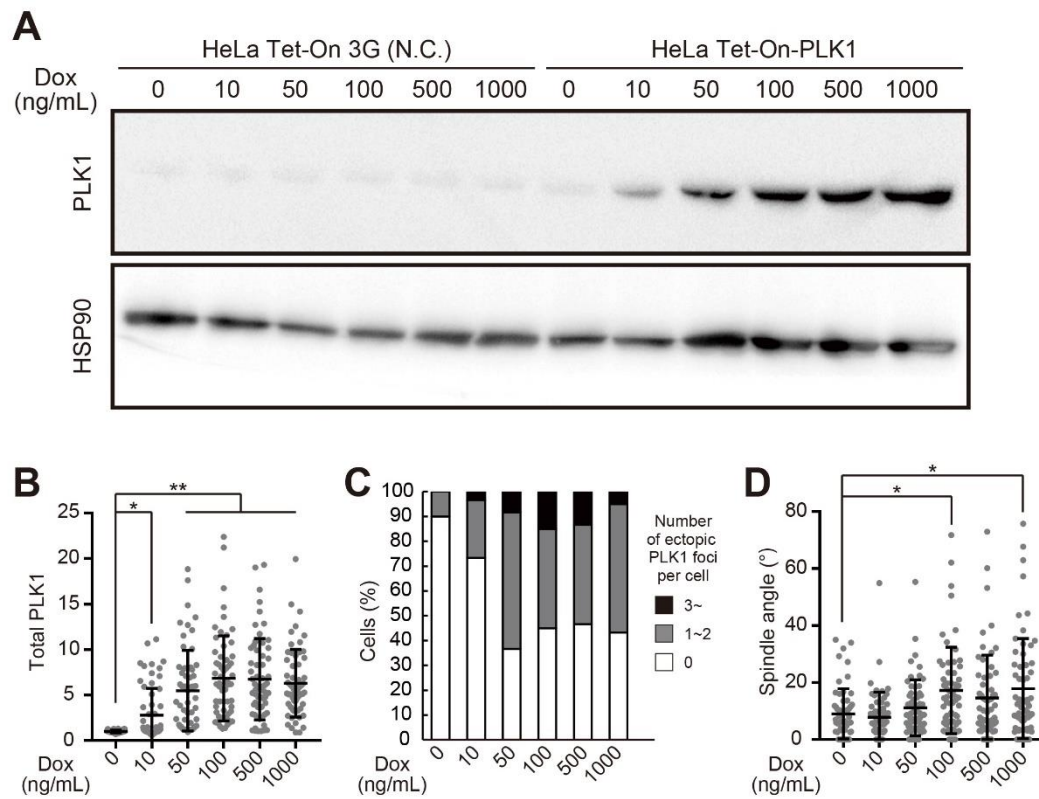
Supplementary Figure 6, Takeda et al.

Figure S6. Titration of doxycycline concentration in HeLa Tet-On-PLK1 cells.

(A) Whole-cell lysates from HeLa Tet-On 3G cells (negative control) or HeLa Tet-On-PLK1 cells treated with various concentrations of doxycycline (Dox; 0, 10, 50, 100, 500, or 1000 ng/ml) were blotted and examined using antibodies against PLK1 and HSP90. (B–D) HeLa Tet-On-PLK1 cells were treated with various concentrations of Dox (0, 10, 50, 100, 500, 1000 ng/ml), and immunostained with antibodies against PLK1 and EB1. (B) The total amounts of PLK1 signal in mitotic cells were quantified by Z-projections (sum of slices) of 41 sections, every 0.5 μm. Line and error bars denote the mean intensity ± s.d. and the Kruskal–Wallis test was used to obtain P values. $N = 60$ cells from two independent experiments ($N = 30$ per experiment). **$P < 0.0001$, *$P < 0.05$. (C) The cells in each group were categorized into three patterns according to the number of ectopic aggregates of PLK1 per cell. In this quantification, the cells selected in (B) were used. (D) Quantification of the spindle angle (°) of the mitotic cells in each group. Positions of spindle poles were judged by the signals of EB1 and PLK1. Line and error bars denote the mean spindle angle ± s.d. and the Kruskal–Wallis test was used to obtain P values. In this quantification, the cells selected in (B) were used. *$P < 0.05$.
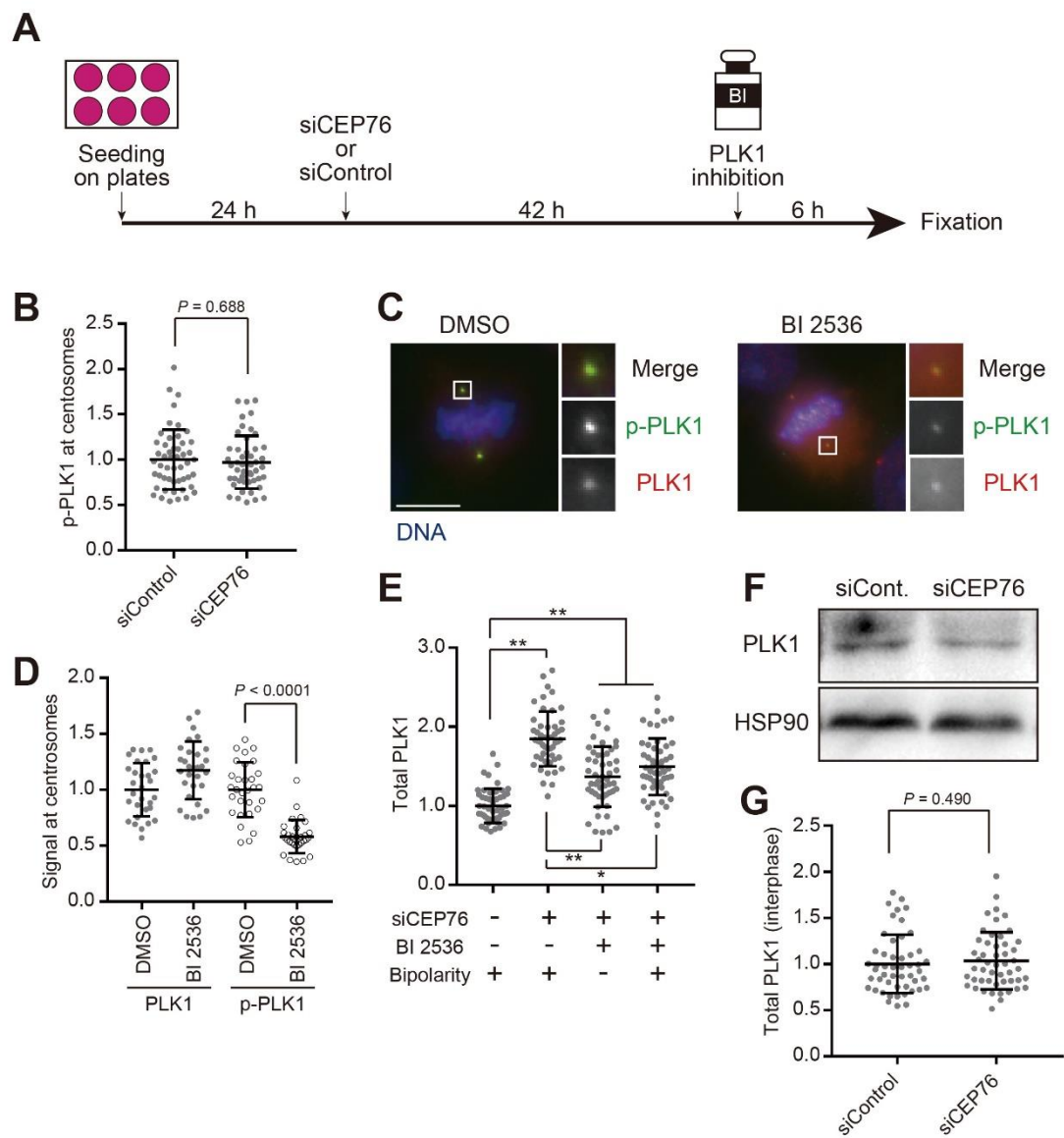
Supplementary Figure 7, Takeda.

Figure S7. Ectopic PLK1 aggregation and spindle orientation defects depending on PLK1 kinase activity in CEP76-depleted cells.

(A) A schematic illustration showing the experimental conditions. Control and CEP76 knockdown cells were treated with DMSO or BI 2536 (a PLK1 inhibitor) for 6 h. (B) Quantification of pT210-PLK1 intensity at centrosomes (PLK1 foci at spindle poles) of the cells in each group in Fig. 5E. Line and error bars denote the mean intensity ± s.d. and the Mann–Whitney U test (two-tailed) was used to obtain P values. $N = 50$ centrosomes. (C, D) HeLa cells were treated with DMSO (0.1%) or BI 2536 (10 nM) for 6 h, and immunostained with antibodies against pT210-PLK1 (green) and PLK1 (red). (D) Representative image of the cells treated with DMSO or BI 2536. Z-projections (maximum intensity) of 21 sections, every 0.5 μm. Scale bar, 10 μm. (D) Quantification of PLK1 and pT210-PLK1 intensity at centrosomes (PLK1 foci at spindle poles) of the cells in each group. Line and error bars denote the mean intensity ± s.d. and the Mann–Whitney U test (two-tailed) was used to obtain P values. $N = 30$ centrosomes. (E) The total amount of PLK1 signal per cell was quantified (Z-projections [sum of slices] of 21 sections, every 0.5 μm). In this quantification, the cells picked up in Fig. 7B were used. Line and error bars denote the mean intensity ± s.d. and the Kruskal–Wallis test was used to obtain P values. $N = 50$ cells from two independent experiments ($N = 25$ per experiment). **$P < 0.0001$, *$P < 0.05$. (F) Whole-cell lysates from control or CEP76 knockdown HeLa cells were blotted and examined using antibodies against PLK1 and HSP90. (G) HeLa cells were treated with siControl or siCEP76, and immunostained with antibodies against GT335 (green) and PLK1 (red). The total amount of PLK1 signal in a cell in interphase was quantified (Z-projections [sum of slices] of 31 sections, every 1.0 μm). Line and error bars denote the mean intensity ± s.d. and the Mann–Whitney U test (two-tailed) was used to obtain P values. $N = 50$ cells.

16

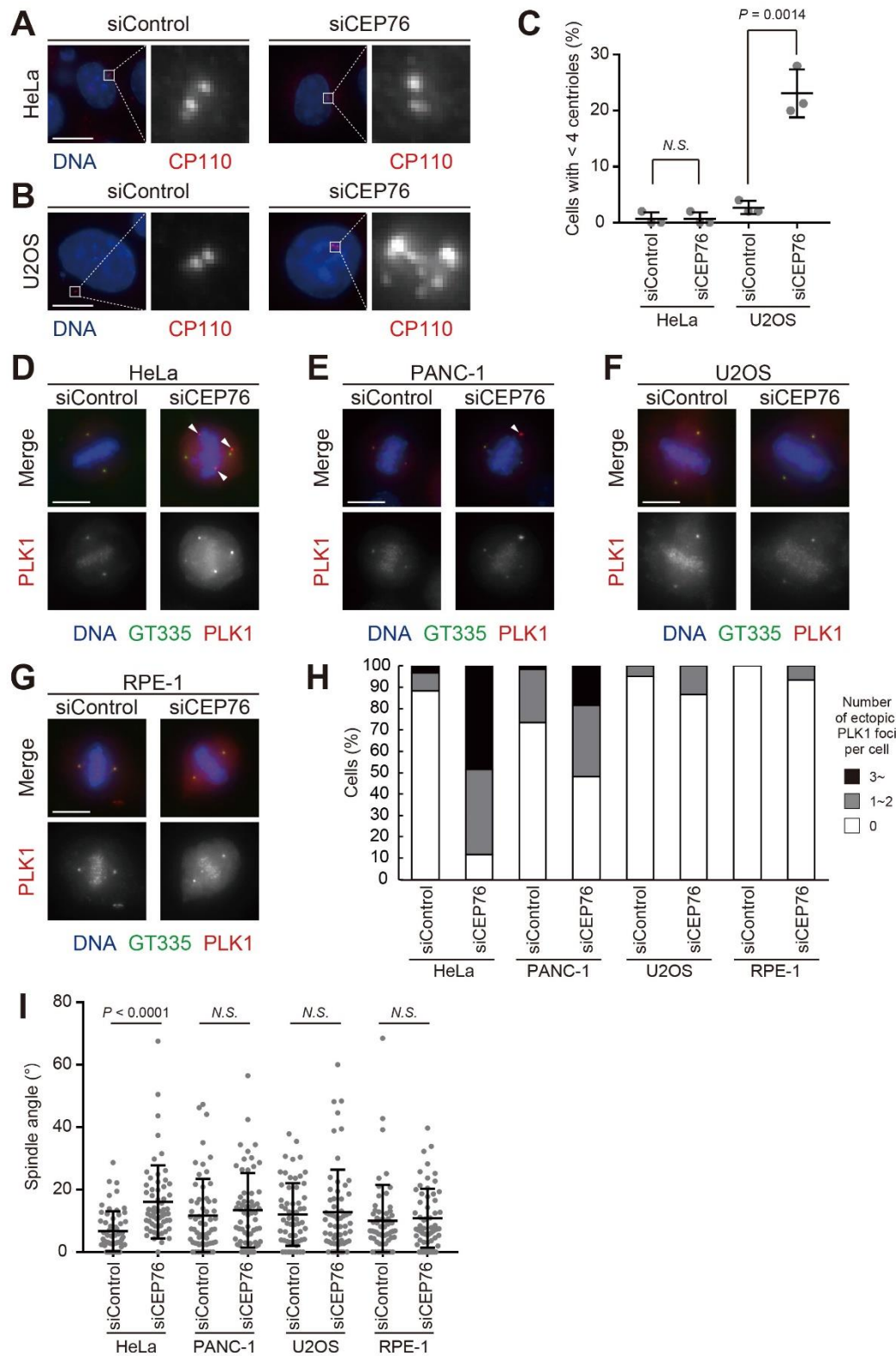## Supplementary Figure 8, Takeda et al.

Figure S8. Comparison of CEP76-depletion phenotypes in several human cultured cell lines.

(A–C) HeLa and U2OS cells were treated with siControl or siCEP76, and immunostained with an antibody against CP110 (red). (A) Representative images of the HeLa cells treated with siControl or siCEP76. Z-projections (maximum intensity) of 21 sections, every 0.5 μm. Scale bar, 10 μm. (B) Representative images of the U2OS cells treated with siControl or siCEP76. Z-projections (maximum intensity) of 21 sections, every 0.5 μm. Scale bar, 10 μm. (C) Frequency of cells with more than 4 centrioles (centriole amplification). The cells in each group in (A) and (B) were used. Line and error bars denote the mean percentage (%) ± s.d. and the unpaired *t* test (two-tailed) was used to obtain *P* values. *N* = 3 independent experiments (47–50 cells per experiment). (D–I) HeLa, PANC-1, U2OS, and RPE-1 cells were treated with siControl or siCEP76, and immunostained with antibodies against GT335 (green) and PLK1 (red). (D) Representative images of the HeLa cells treated with siControl or siCEP76. Arrowheads indicate the ectopic aggregates of PLK1. Z-projections (maximum intensity) of 21 sections, every 0.5 μm. Scale bar, 10 μm. (E) Representative images of the PANC-1 cells treated with siControl or siCEP76. Arrowheads indicate the ectopic aggregates of PLK1. Z-projections (maximum intensity) of 21 sections, every 0.5 μm. Scale bar, 10 μm. (F) Representative images of the U2OS cells treated with siControl or siCEP76. Z-projections (maximum intensity) of 31 sections, every 0.5 μm. Scale bar, 10 μm. (G) Representative images of the RPE-1 cells treated with siControl or siCEP76. Z-projections (maximum intensity) of 21 sections, every 0.5 μm. Scale bar, 10 μm. (H) The HeLa, PANC-1, U2OS, and RPE-1 cells treated with siControl or siCEP76 were categorized into three patterns according to the number of ectopic aggregates of PLK1 per cell. *N* = 60 cells from two independent experiments (*N* = 30 per experiment). (I) Quantification of the spindle angle (°) of all the cells used

in (H). Line and error bars denote the mean angle ± s.d. and the Mann–Whitney U test (two-tailed) was used to obtain P values. $N = 60$ cells from two independent experiments ($N = 30$ per experiment).